DETECTION OF HYPERTENSIVE RETINOPATHY THROUH COLOR FUNDUS IMAGES

A Dissertation submitted in fulfillment of the requirements for the Degree of

MASTER OF ENGINEERING

in

Electronic Instrumentation & Control Engineering

Submitted by

Anju Rani
Regd. No.: 801451001

Under the Guidance of

Dr. DEEPTI MITTAL
Assistant Professor, EIED

2016

Electrical and Instrumentation Engineering Department
Thapar University, Patiala
(Declared as Deemed-to-be-University u/s 3 of the UGC Act., 1956)
Post Bag No. 32, Patiala – 147004
Punjab (India)

DECLARATION

I hereby certify that the work which is presented in dissertation entitled, **"DETECTION OF HYPERTENSIVE RETINOPATHY THROUGH COLOR FUNDUS IMAGES"**, in partial fulfillment of the requirements for the award of the degree of Master of Engineering in Electronic Instrumentation and Control, submitted to Electrical & Instrumentation Engineering Department of Thapar University, Patiala is as authentic record of my own work carried under the supervision of Dr. Deepti Mittal. It refers others researcher's work which are duly listed in the reference section. The matter contained in this dissertation has not been submitted, neither in part nor in full to any other degree to any other university or institute except as reported in text and references.

Place: Patiala
Date: 14-07-2016

(ANJU RANI)

This is to certify that the above statement made by the candidate is correct and true to the best of my knowledge and belief.

(Dr. DEEPTI MITTAL)
Assistant Professor
Electrical & Instrumentation Engineering Department
Thapar University, Patiala

Countersigned By:

(Dr. RAVINDER AGGARWAL)
Professor & Head
Electrical & Instrumentation Engineering Department
Thapar University, Patiala

(Dr. S.S. BHATIA)
Sr. Professor & Dean
Academic Affairs
Thapar University, Patiala

ACKNOWLEDGEMENT

In pursuit of this academic endeavour, I feel that I have been singularly fortunate because inspiration, guidance, direction, cooperation, love and care - all came in my way in abundance and it seems almost an impossible task for me to acknowledge the same in adequate term.

I am very thankful to the Director of Thapar University, **Dr. Prakash Gopalan,** and our Head of the Department, **Dr. Ravinder Aggarwal**, Department of Electrical and Instrumentation Engineering for their support during the research work.

Also, I shall be failing in my duty if I do not record my profound sense of indebtedness and heartfelt gratitude to my supervisor, **Dr. Deepti Mittal**, Assistant Professor, Department of Electrical and Instrumentation Engineering, Thapar University, Patiala, who guided and inspired me in pursuance of this work. It was her able supervision, advice, and guidance from the very early stage of this research as well as giving me extraordinary experiences throughout the work which has resulted in fruitful outcome. I feel bereft of words to acknowledge her contribution to shape my academic perceptivity.

I feel thankful to the entire faculty and staff of the Department of Electrical and Instrumentation Engineering. I would also like to thank my friends who devoted their valuable time and helped me in all possible ways towards successful completion of this work. I thank all those who have contributed directly or indirectly to this work.
Lastly, I would like to thank my parents for their unconditional support and encouragement.

Anju Rani

801451001

TABLE OF CONTENTS

LIST OF TABLES

LIST OF FIGURES

NOMENCLATURE

HR – Hypertensive Retinopathy

CAD – Computer-Aided Diagnosis

AVR – Arteriolar-to-Venular Ratio

DRIVE – Digital Retinal Images for Vessel Extraction

STARE – STructured Analysis of the Retina

INSPIRE-AVR – Iowa Normative Set for Processing Images of the Retina

RET-TORT – Retinal Vessel Tortuosity

FOV – Field Of View

SE – Structuring Element

OD – Optic Disc

ROI – Region Of Interest

DD – Disc Diameter

TP – True Positive

TN – True Negative

FP – False Positive

FN – False Negative

SN – Sensitivity

SP – Specificity

Acc – Accuracy

TPR – True positive rate

FPR – False positive rate

PPV – Positive predictive value

CRAE – Central Retinal Arterial Equivalent

CRVE – Central Retina Venous Equivalent

ABSTRACT

Hypertensive retinopathy is a condition characterized by several pathological changes in the retinal vasculature in response to very high blood pressure. The present work proposes an effective methodology for the detection of hypertensive retinopathy by (i) designing an efficient method to segment blood vasculature and (ii) performing extensive measurements on the segmented blood vasculature to confirm the condition of hypertensive retinopathy.

The proposed vessel segmentation method is designed by rotating top-hat transform at every 22.5° over the entire image to enhance the blood vessels irrespective of their size and direction, and afterwards iterative thresholding is applied on the combination of bit plane slices containing visually significant information related to blood vasculature of a retinal fundus image. The confirmation of hypertensive retinopathy is assured by measuring different diagnostically important performance measures, viz., arteriolar-to-venular ratio, bifurcation points and tortuosity on the segmented blood vasculature. The experimental evaluation of the proposed segmentation method on publicly available databases, viz., DRIVE and STARE shows the accurate extraction of retinal blood vasculature having proximity with the manual segmentation rates provided by the second observer with average accuracy of 94.89% and 94.56% respectively.

The proposed segmentation method and related diagnostic measurements are thoroughly evaluated with four publicly available databases; DRIVE, STARE, INSPIRE-AVR and RET-TORT. The proposed segmentation method and bifurcations are analyzed on two publicly available databases DRIVE, STARE and achieved an average accuracy of 94.89% and 94.56% respectively. The AVR is measured on INSPIRE-AVR with a high accuracy of 97.44%, 98.43% with respect to expert 1 and 2. Various measurements based on curvatures are calculated on the torturous vessels using RET-TORT database. A comparison with several state-of-the-art methods shows that the proposed method represents a significant and competitive improvement in terms of quantitative performance measures.

CHAPTER-1

INTRODUCTION

1.1 Overview

The changes in the retinal vasculature due the prolonged high blood pressure are termed as hypertensive retinopathy (HR). It is one of the leading ophthalmic diseases that affect more than 1 billion of individuals worldwide and accounts for over 20% of deaths among adults [1]. Hypertensive retinopathy is considered as an important modifiable risk factor of disability and mortality in the developing countries whose prevalence is estimated to reach 30% worldwide by 2025 [2]. Hypertensive retinopathy often acts as a silent killer because it does not show any early symptoms, but progressively harms the cardiovascular system. Therefore, the early detection of hypertensive retinopathy is clinically essential for control and prevention of its prevalence with the high blood pressure.

The high blood pressure causes thickening of the walls of retinal blood vessels due to which the blood vessels becomes narrow. The narrowing of retinal blood vessels restricts the blood flowing through the retina which further increases the pressure on blood vessels and optic disc. The various symptoms of HR are arteriolar narrowing, arterio-venous nicking, optic disc swelling (papilledema), haemorrhages (blot, dot, or flame shaped), cotton wool spots and exudates. Fig.1.1 shows retinal images along with the visual symptoms of hypertensive retinopathy. Table 1.1 illustrates classification and grading of HR based on the above symptoms [3].

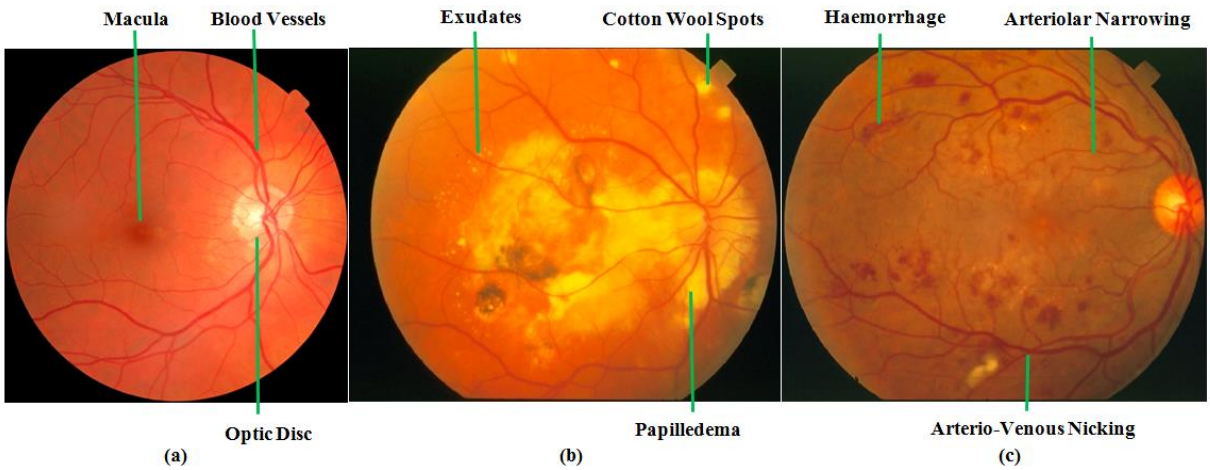

Fig.1.1 (a) Normal retinal image with landmarks; (b) and (c) pathological images showing symptoms of Hypertensive Retinopathy.

Table 1.1. Keith, Wagener, and Barker classification of Hypertensive Retinopathy, based on the level of severity of the retinal changes.

Grade	HR Stage	Symptoms	Features
I	Mild retinopathy	Mild retinal arteriolar narrowing	No detectable signs
II	Moderate hypertensive retinopathy	Mild to severe arteriolar narrowing	Modest association with risk of clinical stroke
III	Mild angiospastic retinopathy	Signs of Grade II plus retinal haemorrhages, hard exudates and cotton wool spots	Strong association with risk of clinical stroke
IV	Severe hypertension	Signs of Grade III plus papilledema	Retinal failure and mortality

The present work focuses on developing a computer-aided diagnosis (CAD) system to aid ophthalmologists in diagnosing hypertensive retinopathy. A CAD system may help ophthalmologists by examining the useful information in fundus images such as retinal vessel abnormalities produced due to hypertension. Therefore, the present work is emphasized on improving methods to detect abnormalities in the retina blood vessels. The accurate extraction of retinal blood vasculature is an important task in CAD of retinopathy. In the last decade, various methods have been developed to automate the segmentation of retinal vasculature in the retinal fundus images. These automated methods can be used to filter out the normal and hypertensive patients therefore reducing the ophthalmologist workload and lead to remarkable cost savings.

Hypertensive retinopathy is detected on segmented blood vessels which require measurements like:

(a) Retinal vessel diameter;

(b) Bifurcation measurements; and

(c) Tortuosity index.

These quantitative measurements are utilized as research tools for the better understanding of relationship between retinal vasculature changes and hypertensive retinopathy.

Arteriolar-to-venular ratio (AVR) **-** The first measure to detect the severity level of hypertensive retinopathy is AVR. Table 1.2 evaluates standard AVR ranges for different grades of hypertensive retinopathy. A normal retina contains no vascular changes with the AVR value ranging from

0.667 to 0.75. Grade I is termed as mild HR where arteriolar narrowing evolve as a major symptom having AVR value from 0.5 to 0.66. Grade II is a term assigned for moderate HR showing symptoms like arteriolar narrowing along with arterio-venous nicking. Its AVR value ranges from 0.33 to 0.5. Grade III shows symptoms like retinal haemorrhages, hard exudates, cotton wool spots, or retinal edema having AVR value in the range of 0.25 to 0.33. Grade IV is the most severe hypertension that may lead to mortality having AVR value less than 0.2.

Table 1.2. The range of AVR for different grades of HR according to the severity level

Grade	**AVR**	**Symptoms**
Normal	0.66-0.75	No vasculature change
Grade I	0.5-0.66	Mild compression of venules
Grade II	0.33-0.5	Compression or elevation of venules
Grade III	0.25-0.33	Arterio-venous nicking, retinal haemorrhages, exudates and cotton wool spots
Grade IV	<0.2	All symptoms mentioned above along with papilledema

Bifurcations - The high blood pressure causes changes in geometrical attributes of blood vessels such as angle and diameter in all blood vessel segments. Any change in the branching geometry of retinal vasculature leads to increased power requirement for transporting blood throughout retina. The changes can be observed by the modification of bifurcation which may be used as an indication of illness in progress. Therefore, the identification of vascular bifurcations is one of the basic steps in this analysis [4]. A normal retinal fundus image consists of more than 100 vascular bifurcations [5].

Tortuosity - It is defined as abnormal elongation of the blood vessels due to prolonged high blood pressure and since the end points of the vessels are fixed, therefore the extra length will twists and form curves [6,7]. It is assumed that increase in number of curvature changes leads to more tortuous vessels. Tortuosity in the retinal images is observed to be higher in vessels having smaller width than the vessels having larger width. Similarly, increase in the amplitude of vessel segment leads to the increase of vessel tortuosity associated with it. Fig.1.2 depicts a tortuous retinal image from RET-TORT database.

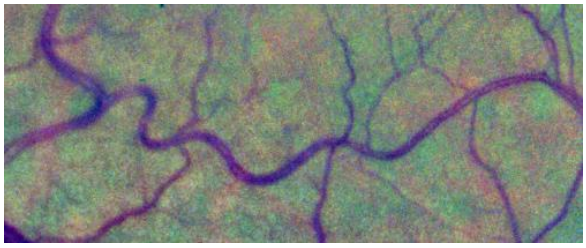

Fig.1.2 An example image from the RET-TORT database.

1.2 Motivation and Main Contribution

It has been well known that hypertension causes changes in retinal blood vasculature. The manual estimation of changes in the appearance of retinal fundus images is too subtle to be detected by ophthalmologists. Therefore, automatic/semi-automatic methods are necessary to detect retinal vascular changes due to hypertension. These methods when included in the designing of computer aided diagnosis (CAD) have substantial impact on clinical practice and may lead to an improved assessment for the patients at a risk of hypertensive retinopathy.

The proposed method focuses on early detection of hypertensive retinopathy through automatic identification and evaluation of vasculature changes. The accurate estimation of retinal vascular changes is a challenging task and requires optic disc detection, vessel segmentation, vessel map analysis, retinal vessel diameter measurements, artery-vein discrimination, bifurcations and measurement of torturous vessels. Therefore, the present work proposes an extensive methodology to segment retinal blood vessels and evaluation of HR on four publicly database viz. DRIVE, STARE, INSPIRE-AVR, RET-TORT.

The proposed segmentation method is designed by combining top-hat transform and bit plane slicing on DRIVE and STARE databases with the objective that the designed segmentation method can easily remove segmentation errors produced due to the boundary of blood vessels and optic disc. The top-hat transform is able to adapt changes in the vessel width and orientation of vessels caused due to hypertension by using a structuring element that orients over the entire image to enhance blood vessels at each direction. The bit plane slicing will further help in determining the most significant information of the blood vessels. This information is necessary for accurate diagnosis of HR by measurements like AVR, bifurcations and tortuosity.

The AVR measurement is evaluated on INSPIRE-AVR database to validate the performance of the proposed method with respect to the observers. To provide a generalized measurement for bifurcation properties, sufficiently large number of vessel segments is required. Therefore, thinning operation is applied on the proposed method to obtain single pixel width for 643 bifurcation segments from DRIVE and STARE. The deviation of the bifurcation properties for

pathological images to normal images has been discussed in detail. Similarly, the tortuosity measurements are calculated for a standard database RET-TORT to give a brief comparison between various methods proposed by the researchers for hypertensive and normal retinal images. The proposed system is steadfast, proficient and provides definitive results. The automated method proposed may aid medical professionals in important clinical judgments and provides better performance in terms of accuracy and time.

1.4 Thesis Overview

This thesis is organized in the following main sections. Chapter 2 gives a brief literature review of previously proposed methods. Chapter 3 describes the materials and methods used in the proposed methodologies. Also, the measurements of vascular changes due to hypertensive retinopathy have been discussed in details. Chapter 4 discusses the experimental results of the proposed method and Chapter 5 illustrates discussions on the key findings and Chapter 6 concludes of the thesis along with the scope for future research in this area.

The methodology of proposed system includes automated blood vessel segmentation, optic disc and ROI detection, arteries and veins discrimination and the measurements of vessel parameters such as AVR, bifurcations, tortuosity index on various publicly available databases for the early diagnosis of hypertensive retinopathy.

CHAPTER-2

LITERATURE REVIEW

The segmentation of retinal blood vessels is an important aspect of any medical decision support system or CAD system. Table 2.1 illustrates various automatic/semiautomatic methods proposed by several researchers which provide satisfactory results in some cases, still leave room for improvement in the vessel segmentation, especially in abnormal retinal images. The following section focuses particularly on the methods proposed by various researchers for the extraction of blood vessels from retinal images acquired from a fundus camera.

2.1 Retinal Blood Vessel Segmentation

The matched filtering technique was proposed by Chaudhuri et al. [8] and later adapted and extended by Hoover et al. [10]. However, this method failed to detect the junction points and small vessels segments. Chakraborti et al. [38] proposed self-adaptive matched filter and achieved accuracy of 93.7% and 93.79% for DRIVE and STARE databases respectively. Although, matched filter was used by number of researchers producing an image of good quality, satisfying for the large vessels but were partially able to detect small vessels of poor contrast. It also results in some false detection of blood vessels therefore; it may be difficult to separate the vessel structures from the false detection. The top-hat transform has been used in combination with various morphological operators in order to get the accurate retinal vasculature. Zana and Klein [11] segmented the retinal vasculature using top-hat transform along with mathematical morphology. The idea behind their method was to automatically segment the vessels using shape, connectivity, as well as differential properties like curvature. But the method fails to detect vessels having low contrast and achieved accuracy of 93.77% on DRIVE database. This kind of segmentation was used for image registration of retinal images where connectivity is used for feature calculation. Yang et al. [21] proposed a combination of top-hat transform and fuzzy clustering algorithm to reduce the weak edges and noise to obtain better segmented blood vessels. The method achieved a high accuracy ratio of 95.2% on STARE database. Muramatsu et al. [28] proposed a combination of top-hat transformation and double-ring filter to extract the retinal vasculature and automated calculation of AVR. Rossant et al. [33] proposed a combination of a top-hat transform with linear filters. The segmented retinal vasculature was obtained by using automatic thresholding technique and achieves an accuracy of 94.33% on DRIVE database. Xu et

al. [35] proposed a method in combination with top hat transform and shape-based morphology to segment the retinal blood vessels. The proposed method achieves an accuracy of 94.47% and 94.71% on DRIVE and STARE databases respectively.

Table 2.1 Summary of previous research works related to retinal blood vessel segmentation.

Ref. No.	Year	Vessel segmentation Method	Performance Measures		Prons	Cons
			DRIVE	STARE		
[8]	1989	2D Gaussian matched filter	Acc=0.8773	-	Use of simple enhancement, thresholding operators	Large computational time
[9]	1999	Region growing algorithm	SN=0.785 SP=0.949 Acc=0.932	-	Overcomes the problem of contrast inherent variations	Low sensitivity
[10]	2000	Matched Filtering, Threshold probing	-	SN=0.6751 SP=0.9567 Acc=0.9267	Proposed new method	Used database of five images
[11]	2001	Top hat transform, Cross curvature evaluation	SN=0.6971 Acc=0.9377	-	Can be used for image registration	Background structure remains noisy
[12]	2003	Adaptive local thresholding	SN=0.659 SP=0.96 Acc=0.928	-	Simplicity of the method allows it to be applicable on a variety of other tasks	Pruning operation takes about 70% of the computation time
[13]	2004	Laplacian profile model	-	SN=0.924 SP=0.921	Useful for vessels that split due to specular refection	Low specificity
[14]	2004	Morphological bit plane slicing	SN=0.7344 SP=0.9764 Acc=0.9452	SN=0.6996 SP=0.9730 Acc=0.9440	Used color features for segmentation	Poor results with vessel having light reflex
[15]	2006	DOG filter, Multiscale morphological reconstruction	Acc=0.9535	-	Low computational time of 2.5 min	Unable to remove background noise
[16]	2007	Improved Gaussian			Improved responses	

		matched filter	SN=0.7246 SP=0.9655 Acc=0.9344	SN=0.7506 SP=0.9569 Acc=0.9410	for matched filter	Limited to find filter Parameters
[17]	2007	Maximum principal curvature, Gradient magnitude, Region growing	SN=0.660 SP=0.9612 Acc=0.9220	SN=0.779 SP=0.9409 Acc=0.9240	Automated technique	Unable to eliminate Abnormalities
[18]	2007	ITK serial implementation	SN=0.780 SP=0.978	SN=0.752 SP=0.980	Improved computational Efficiency	Unable to handle high resolution images
[19]	2007	Multiresoution Hermite model	SN=0.6634 SP=0.9682 Acc=0.9316	-	New algorithm is proposed	No measurements Performed
[20]	2007	Snake algorithm, Topological properties	-	Acc=0.952	Good for localization of optic disc	Low sensitivity due to un-segmented thin vessels
[21]	2008	Top hat transform, Fuzzy clustering	Acc=0.9419	-	High accuracy and low misclassification	Low connectivity
[22]	2008	Scale space analysis Parameter search	-	Acc=0.94	Good trade-off between quality and processing speed times	Poor results for pathological Images
[23]	2008	Multiscale Line Operator, Region growing	-	Acc=0.9474	Found good estimate of vessel width	No fine vessels detected
[24]	2008	Divergence of vector fields	SN=0.7436 SP=0.9615 Acc=0.9352	-	High accuracy	Did not discussed dark Abnormality
[25]	2008	Snakes algorithm, Morphological processing	SN=0.747 SP=0.955 Acc=0.929	-	Good results in arterio-venous structures	Low sensitivity

[26]	2009	Multiscale line tracking	SN=0.7282 SP=0.9551	SN=0.7521 SP=0.9681	Fast tracking process	Misclassification of optic disc
[27]	2009	Ribbon of Twin active contour model	SN=0.793	-	Accurately locate vessel edges in close vessels, light reflex	Low specificity
[28]	2010	Top-hat transformation, Double-ring filter	-	SN=0.7000 SP=0.9530	Automated segmentation and classification	Segmentation method can be Improved
[29]	2010	Maximum likelihood estimation of scale space parameters	Acc=0.92	-	Estimates vessel parameters directly from image rather than binarized image	Low true positive value
[30]	2010	Phase Concurrency, Log-Gabor filter	SN=0.744 SP=0.966 Acc=0.943	-	very low computational time of 10sec	Low accuracy
[31]	2010	Vessel tracing algorithm	SN=0.7352 SP=0.9795 Acc=0.9458	-	High accuracy for vessel segmentation and diameter estimation	Low sensitivity
[32]	2011	Curvelet transform, Multi-structure elements morphology by reconstruction	SP=0.9788 SP=0.7031 Acc=0.9433	-	High sensitivity of multistructure elements provides better segmentation	Needs proper thresholding algorithm to find small vessels
[33]	2011	Top hat transform, Automatic thresholding	SN= 0.7224 SP=0.9711 Acc=0.9469	-	Automated method results in high specificity	Cannot detect narrow vessel Extremities
[34]	2012	Gabor filter, Morphological transformations	TP=0.6924 TN=0.9779 Acc=0.9413	TP=0.7149 TN=0.9749 Acc=0.9471	Used orientation analysis of gradient vector field and obtained good results	Poor segmentation due to bright central reflex
[35]	2013	Top hat transform, Shape-based	Acc=0.9461	Acc=0.9501	Simple filtering and segmentation	Constrained

		morphology				vessel connectivity
[36]	2013	Multiscale hierarchical, decomposition Adaptive thresholding	TPR=0.7512 FPR= 0.0316 Acc=0.9412	TPR=0.7887 FPR=0.0367 Acc=0.9441	Generates competitive results in terms of accuracy	Non-classification of arteries and veins
[37]	2014	Graph cut technique	SP=0.9579 SN=0.7205 Acc=0.9370	SP=0.9586 SN=0.6786 Acc=0.9379	Good results for vessel segmentation and optic disc detection	Suffers from overlapping tissue Segmentation
[38]	2014	Self-adaptive matched filter	SN= 0.8173 SP=0.9733 Acc=0.9767	SN=0.8104 SP=0.9791 Acc=0.9813	High accuracy	Low sensitivity
[39]	2015	Gaussian filtering, Simple Linear Iterative Clustering	Acc=0.9332	Acc=0.8600	Automated method	High computational time of 120min
[40]	2016	Gabor Wavelet filter, Frangi's filter	Acc=0.9332	Acc=0.8600	Better responses compared to single filter	False positive in areas close to Border

*SN-Sensitivity, SP-Specificity, Acc-Accuracy, TPR- True positive rate, FPR- False positive rate

2.2 Arterio-to-Venular Ratio

The estimation of AVR is a challenging task and requires optic disc detection on the segmented blood vessels. Optic disc detection is necessary to determine the region of interest (ROI) where the vessel measurements are carried out. A semi-automatic method using Gabor wavelet and morphological operations was proposed by Ortiz et al. [41]. The method was tested on clinically acquired database of 30 images with 57% accuracy. Narasimhan et al. [42] proposed blood vessel detection method using top hat transform on 76 retinal images of VICAVR database and 25 images that were clinically acquired. Inspite using a large dataset, limited information is provided in terms of AVR values. Agurto et al. [43] presented a vessel segmentation method based on multi-scale linear structure enhancement and the second order local entropy thresholding. The method was tested on 74 fundus images with 80% accuracy. The AVR calculation was carried out

on (0.5-1) optic disc diameter (DD) which may give inappropriate results. Ruggeri et al. [44] presented a vessel tracking algorithm on 50 clinically acquired images. But some of the vessels were missed by the tracing procedure therefore gave unsatisfactory AVR values. Manikis et al. [45] presented a hessian based vessel segmentation method along with thresholding and achieved an accuracy of 93.71% and 93.18% for DRIVE and STARE respectively. In AVR calculation, region of interest (ROI) is highly dependent on optic disc detection but they did not provided a clear idea of optic disc detection method which was used in their work. Muramatsu et al. [46] presented a method for retinal blood vessel segmentation, classification and selection of arteries and veins, optic disc segmentation along with AVR. The sensitivity for classification of arteries or veins was found to be 87%, while 93%. Khitran et al. [47] presented a new method of AVR computation. They tested their method on 58 fundus images of VICAVR and 40 images of DRIVE database and achieved an accuracy of 96.5% and 98% respectively. The limitation of their work was that sufficient description of their results is not presented by them. Li et al. [48] presented an automated method to calculate AVR, but the method still required few user inputs to detect arteries and veins.

2.3 Bifurcation Features

Apart from the changes in the retinal vascular diameters due to high blood pressure, research has recently focused on the quantitative estimation of other signs of retinal vascular geometry, such as the bifurcation of the retinal vessels. Several methods have been proposed in order to measure bifurcation features. Azzopardi et al. [4] uses a set of combination of shifted filter responses to detect the vascular bifurcations automatically in the segmented retinal images. But, incomplete bifurcations were a commonly problem by this automatic segmentation technique. Perez et al. [5] proposed a geometric feature based technique for detecting vascular bifurcations based on skeletonized retinal vasculature. They characterize the bifurcation by the total number of intersections using a fixed-size circular window centered on the candidate landmark points. But it fails when two bifurcation points are very close within the window. This process also gives false identification of landmarks when another vessel passes through the fixed-size window. Chapman et al. [49] determined the changes in arteriolar diameters at branch points due to prolonged stress across the arterial networks. This study aims at determining the affect of stress on the retinal bifurcations. Shen et al. [50] and Tsai et al. [51] proposed model based approaches to detect bifurcation points. But these methods suffer from insufficient to detect typical bifurcations. Diri et al. [52] made manual measurements of bifurcations by placing a rectangle on vessel segments to measure width. The measurements were done on 230 bifurcations from the DRIVE database. But

to provide more meaningful results, vessel segmentation along with bifurcation detection technique should be discussed. Abbadi et al. [53] detects 100 vascular bifurcations from the retinal vascular by removing it from the images using specific mask. To provide a generalized measurement Shen et al. [54] and Chanwimaluang et al. [55] proposed cross perpendicular structures and Y-type structures with eight connected neighbors for the extraction of vasculature and detect bifurcations based vessel centre-line. But these methods may tend to wrongly detect the bifurcations due to the error produced by skeletonization process due of abrupt change of the width of any vessel within the mask window.

2.4 Tortuosity Features

The detection of retinal vascular tortuosity may be considered as an evidence for early indication of micro vascular damage in patients with hypertension. Nidhal and Enas [56] proposed arc-to-chord ratio to measure retinal vascular tortuosity. But the proposed algorithm was not effective for the curved vessels. Onkaew et al. [57] proposed chain code algorithm to measure tortuosity on each vessel segment employing number of curvature inflection points. Zhou et al. [58] utilizes the method of integral curvature along a blood vessel a method to distinguish between tortuous and non-tortuous blood vessels. Kaupp et al. [59] presented an automated tortuosity measurement based on Fourier analysis of blood vessels along its perpendicular. Smedby et al. [60] describes tortuosity measures depending on the integral curvature and number of inflection points of the blood vessels. Capowski, Kylstra and Freedmen [61] presented the measurement of tortuosity index based on spatial frequencies.

The general limitation of the above methods is: (i) under-segmentation and over-segmentation of blood vessels; (ii) moderate performances of segmentation in terms of sensitivity, specificity and accuracy; (iii) inaccurate optic disc detection; (iv) bifurcation measurements on limited dataset, and (v) comparative study of tortuosity on a standard database.

In the present work, an attempt has been made to overcome all the above limitations. A new automated segmentation method is developed which includes benefits of top-hat transform and bit plane slicing to obtain accurate retinal vasculature. The proposed method provides better results than the methods discussed in literature for both DRIVE and STARE databases. The accurate detection of optic disc is carried out using circular hough transform. The optic disc is necessary to locate the region of interest for AVR calculation. The detection of bifurcation points and tabulation of the geometrical measurements are evaluated on 643 bifurcations from DRIVE and STARE databases. Tortuosity measurements using various methods are evaluated and compared on a standard RET-TORT database of 60 images.

The major highlights of the method are its validation on larger and standard databases resulting in comparatively higher sensitivity, specificity and accuracy than other methods discussed in the literature, accurate blood vessel segmentation for the early detection of hypertensive retinopathy.

The methods comprises of three phases: (i) pre-prosessing through morphological operators, top hat transform in combination with bit-plane slicing (ii) retinal blood vessel segmentation using iterative thresholding (iii) post-processing measurements like AVR, bifurcation measurements, tortuosity index.

CHAPTER-3

MATERIALS AND METHODS

3.1 MATERIALS

The present work is evaluated on five publicly available databases namely Digital Retinal Images for Vessel Extraction (DRIVE), STructured Analysis of the REtina (STARE), INSPIRE-AVR (Iowa Normative Set for Processing Images of the Retina), MESSIDOR and RET-TORT (Retinal Vessel Tortuosity). The DRIVE and STARE database is used for vessel segmentation, INSPIRE-AVR and MESSIDOR for validating the results of AVR while the RET-TORT database is used for measuring tortuosity.

(a) DRIVE database

The DRIVE database consist a total of 40 retinal color fundus images [62]. Out of these 40 images, seven images are pathological images containing lesions like exudates, hemorrhages and pigment epithelium changes. These images were acquired using a Canon CR5 non-mydriatic 3-CCD camera with a 45° field of view (FOV). Field of view is the angle over which the retinal fundus image is recorded. Each image of the DRIVE database is captured with a resolution of 768 × 584 pixels. The availability of ground truth and expert's opinion regarding blood vessel segmentation is useful in comparing the results of proposed method.

(b) STARE database

The STARE database consists of 20 images for retinal blood vessel segmentation [63]. Out of these, 10 images are normal while 10 are pathological images. The digital images were captured by a TopCon TRV-50 fundus camera at 35° field FOV. Each image in the STARE database is captured with a resolution of 605×700 pixels. The STARE database provides manually segmented images by two observers which may help in evaluating the performance of proposed method.

(c) INSPIRE-AVR database

The INSPIRE-AVR database consists of 40 retinal blood vessel images along with the reference standard of AVR [64]. The reference standard is provided by two experts using IVAN, which is a semi-automated computer program. An AVR reference standard provided by two experts is used for the assessment of AVR results of the proposed method.

(d) MESSIDOR database

The MESSIDOR database consists of 50 retinal images showing different vasculature [65]. This variety can be helpful to assess the generalized performance of the proposed method. The images were captured using 8 bits per color plane at 1440×960, 2240×1488 or 2304×1536 pixels.

(e) RET-TORT database

The RER-TORT database contains a total of 60 retinal vessels images from normal and hypertensive patients [66]. These images are arranged in two sets, each containing 30 images of retinal arteries and veins of similar vessel length and width. The images in the dataset were acquired by a TopCon TRC 50 fundus camera at 50° FOV. Each image in the dataset is captured with a resolution of 1100x1300 pixels. The database also provides information about the tortuosity measurement provided by an expert.

3.2 METHOD – 1

In the present work, a new simplified method is designed to extract retinal vasculature structure using dual top hat transform. The flowchart of the proposed method is depicted in fig.3.1 and explained in the following paragraphs.

3.2.1 Pre-processing

Preprocessing is the low level abstraction of images. It aims to suppress the unwanted distortions and enhance the features of images which are important for further processing. Therefore, the retinal color fundus image is pre-processed in this work. A retinal color fundus image is made up of green, red, and blue channels. Amongst them, green channel is selected because of better contrast and more information than the other two channels. The high resolution fundus images often have a central light reflex (light streak) formed due to reflection from the interface between the blood column and vessel wall. Due to this, the arterial wall turns so opaque that the blood column becomes invisible and the central reflex occupies the entire width of the arteriole. Therefore, the green channel is filtered to fill any gaps in the vessels which may introduce errors during segmentation. It is done by applying a morphological opening with a disk of radius 1 pixel as the structuring element (SE). The intensity variation in the background of the retinal fundus images suffer from non-uniform illumination which is removed by obtaining a homogenized image. The output image obtained has better contrast in comparison to the green channel image.

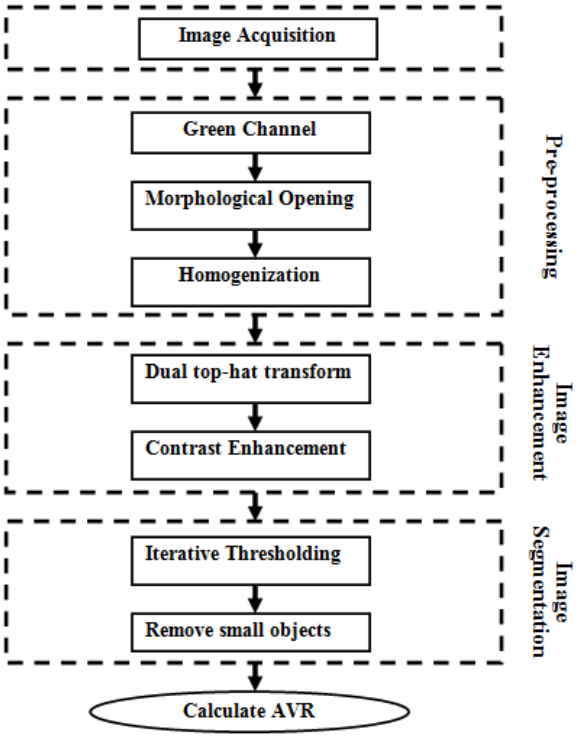

Fig. 3.1 Flowchart of the proposed method -1.

3.2.2 Vessel Enhancement

After preprocessing, a complementary image of the homogenized image is taken to get enhanced visualization of the vessels in the image. To extract the blood vasculature, morphological dual top-hat transform is applied using a disk as structuring element of eight pixels in radius. The size of the SE used in dual top-hat transform should be chosen according to the size of the desired object. The bigger the SE, the larger the object extracted. There are some dark features like blood vessels, fovea, micro aneurysms or hemorrhages that may produce reflection artifacts. The dual top-hat transform remove these reflection artifacts while preserving the dark features like blood vessels in the image. These blood vessels are required for the computation of arteriolar to venular ratio. The dual top hat transform does not preserve the shape of the objects precisely. Therefore, dilation is performed to preserve the shape of the blood vessels and filter the objects that have size less than the SE.

3.2.3 Vessel Segmentation

Accurate segmentation of retinal blood vessels is essential to achieve precise calculation of AVR measurement. An iterative thresholding method is applied in this work for segmenting the retinal vasculature. A binary map of vessels is obtained at the end of this step. In the retinal

images, veins are usually dark and wide while the arteries are bright and thin. After finding the retinal vasculature, the intensity variation is used to classify the retinal vessels as arteries and veins.

3.3 METHOD – 2

The following section describes the proposed method for detection of hypertensive retinopathy through retinal blood vessel segmentation and vessel measurements on color fundus images. The method-2 is an improvement of the above discussed method-1 in terms of vessel segmentation on which number of quantitative measurements is carried out for the detection of hypertensive retinopathy. Fig.3.2 illustrates the modules involved in the proposed methodology.

3.3.1 Proposed Vessel Segmentation Method

The retinal color fundus images usually contain additive and multiplicative noise at the background during acquisition, which may cause difficulties in the accurate extraction of blood vasculature. Therefore, the removal of noise is essential for the accurate segmentation of the retinal vasculature. A retinal color fundus image consists of green, red, and blue channels. Amongst them, green channel is chosen because it has the highest contrast between background and blood vessels along with the information regarding different anatomic structures of the retina [67, 68].

(a) Removal of central light reflex

The high resolution fundus images often have a central light reflex (light streak) which runs along the centre of the blood vessel [69]. The light streak may occupy the entire width of the blood vessel creating gaps in between blood vessel or making it entirely invisible. Therefore, the green channel is filtered to remove the central light reflex which may introduce errors during segmentation. It is done by applying a morphological opening with a linear structuring element of length 8 pixels. The blood vessels have small curvatures therefore, they are assumed to be piecewise linear having Gaussian shape profile. Due to piecewise linear nature of vessels, morphological filters with linear structuring elements are used to enhance the vessels in the retinal image. The length of structuring element is selected such that it should merge the gaps present within the vessels but should not merge the vessels that are close to one another.

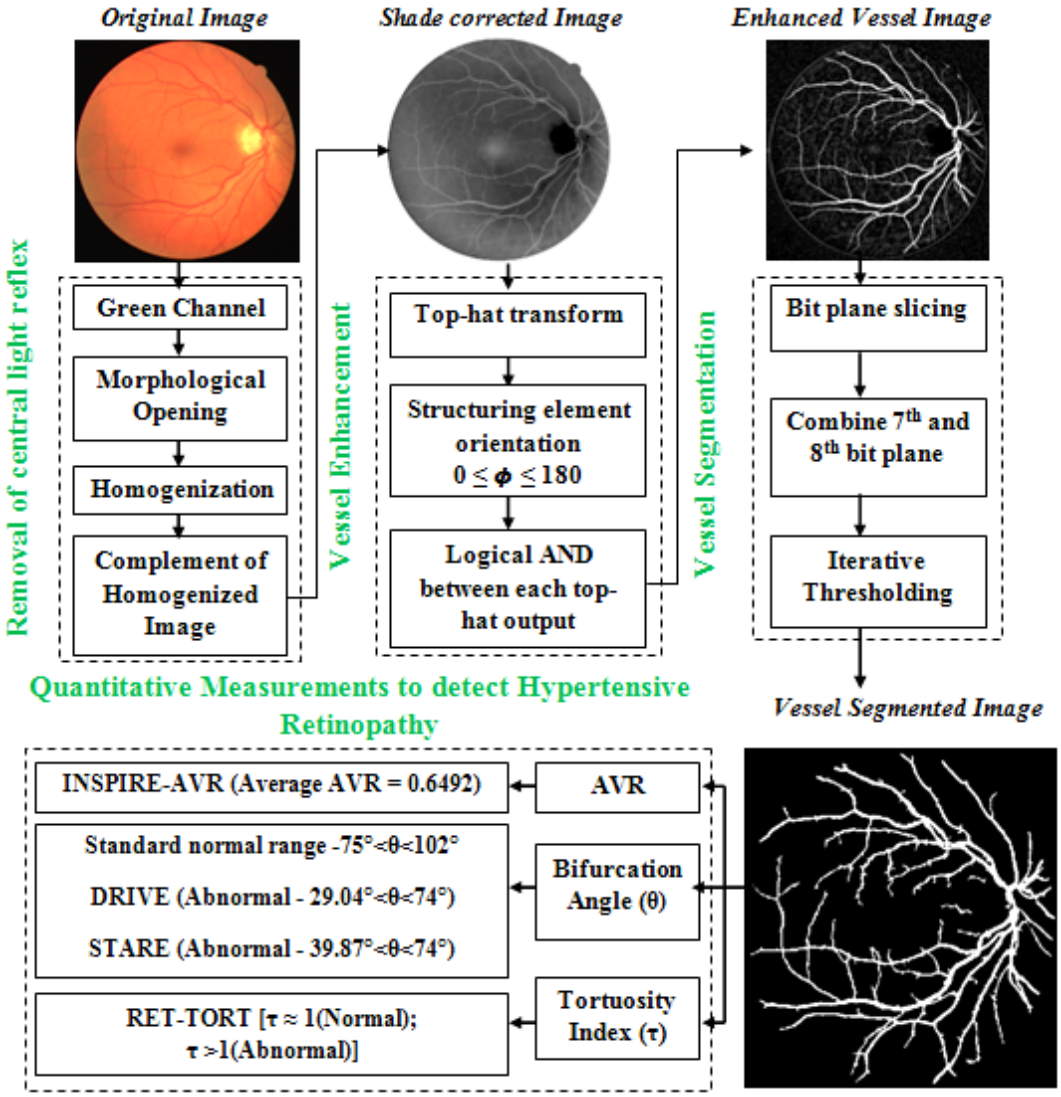

Fig.3.2 Flowchart of the proposed method- 2.

The opening operation helps in filtering the retinal vessel by erasing the objects from the green channel which have smaller size then that of the structuring element used. The output image obtained by morphological opening still has intensity variation at the background. This non-uniform illumination is removed by obtaining a homogenized image. The contrast between blood vessels and background is improved by taking a complement of the homogenized image. Thus, the image obtained has better contrast in comparison to the green channel image but still small vessels with low contrast are not visible clearly. Therefore, there is a need of vessel enhancement.

(b) Vessel Enhancement

Vessel enhancement is an important step for the projection of maximum intensity which improves the contrast of small vessel and helps in the accurate reconstruction of the retinal vasculature. Here, the vessel enhancement is performed using top hat transform with different

orientations of the linear structuring element. The morphological top hat transform is shown in eq. (3.1)

$$I_{tophat}^{\phi} = \left[I - \left(I \; o \; S^{\phi} \right) \right] \tag{3.1}$$

where, I_{tophat}^{ϕ} denotes the output image obtained by top-hat transform, I is the input image to be processed, S is the 'line' structuring element, ϕ is different angular orientations of the line structuring element and $\left(I \; o \; S^{\phi} \right)$ denotes morphological opening of image I with each structuring element having different orientation.

The line structuring element used for the opening is a matrix representing a line with 21 pixels of length and rotated at every 22.5°. The largest possible diameter of the retinal vessel is chosen as the size of the line structuring element. It was observed that the retinal vessels may be oriented at any angle ϕ such that ($0 \leq \phi \leq \pi$). Therefore, the structuring element must be rotated in order to extract the retinal vessels present at different orientations. Fig.3.3 shows the output vessel images obtained by rotating the structuring element at 15°, 22.5°, 30°, 37.5 and 45°. Therefore, experimentally it was found that performing the opening operation along line structuring element by rotating it at 22.5° will extract all the vessels present in each direction. Finally, the sum of top-hat transform along each direction is obtained as depicted in eq. (3.2),

$$S_{tophat} = \sum_{\phi=0}^{180} \left(I_{tophat}^{\phi} \right) \tag{3.2}$$

where S_{tophat} is the sum of top-hat transform performed with different orientations.

The output image obtained by this method helps to remove every isolated round and bright zone whose diameter is less than the length of the linear structuring element. Therefore, the sum of top-hat transform on the filtered image will enhance all vessels regardless of their direction, including small or tortuous vessels. The output image obtained from the sum of the top-hat transform operation is a monochromatic grayscale in which the gray levels are distributed in such a way that the blood vessels are highlighted more than the background. This 8-bit gray scale image can be represented in the form of bit planes, ranging from the least significant bit plane 1 to most significant bit plane 8. Therefore bit plane slicing is used to determine the bit planes that contribute significant information.

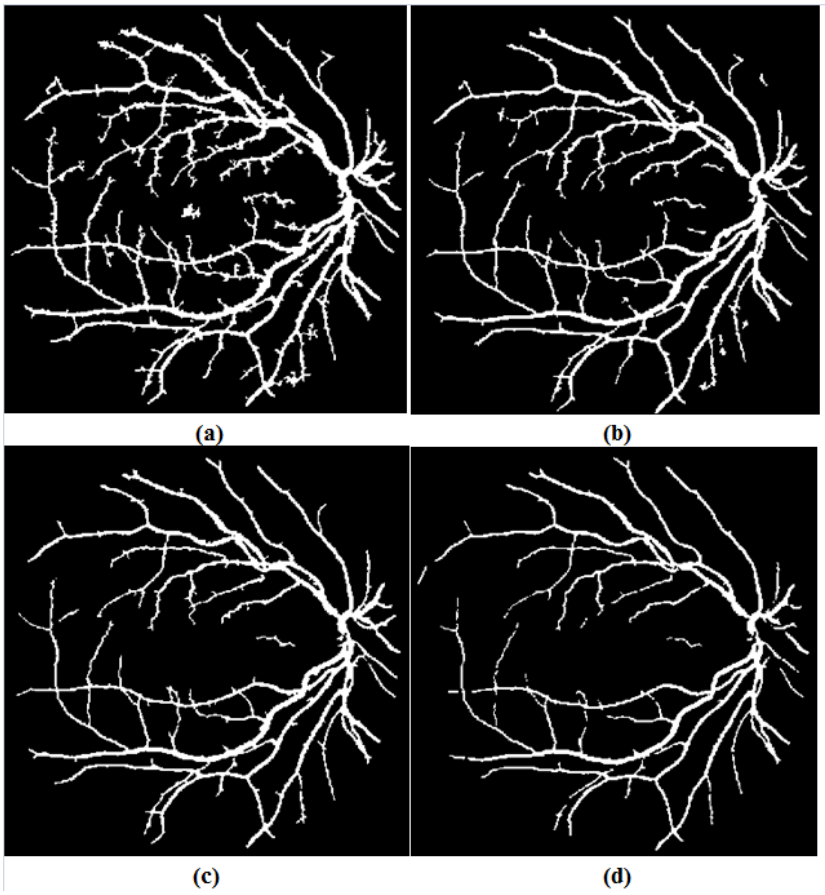

Fig.3.3 Output images of segmented vasculature obtained by rotating the structuring element at (a) 15°, (b) 22.5°, (c) 30° and (d) 45°.

Bit plane slicing is the contribution of specific bits on the total image appearance. Separating a digital image into its bit planes is useful for analyzing the relative importance played by each bit of the image. It is due to the fact that the intensity of an image at specific pixel is represented by 8 bits therefore there will be eight such planes. It is observed that the higher order bits, especially the bit plane 7 and bit plane 8 contain the majority of the visually significant data while bit plane 1 to 6 appears as noise. Fig.3.4 shows 8 bit planes obtained by bit plane slicing of the vessel enhanced image. Finally, a single binary image is obtained by taking the sum of bit plane 7 and bit plane 8. Therefore, the image obtained after performing top hat and bit plane slicing is the approximation of the shape and orientation map of the retinal blood vessels. The final step is to obtain a binary image for the calculating the vessel measurements.

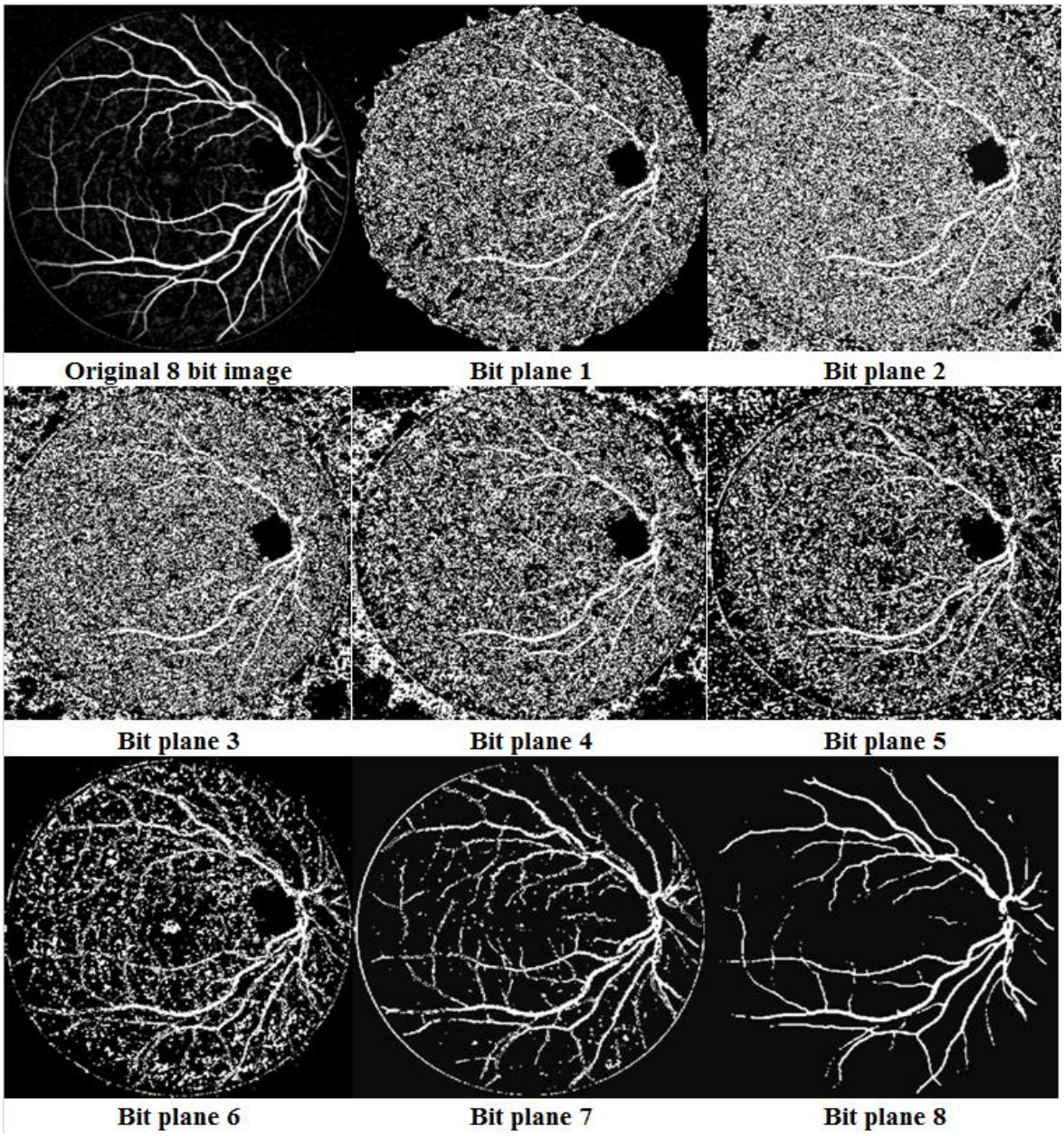

Fig.3.4 Image illustrating the output of bit-plane slicing for all eight planes

(c) Vessel Segmentation

The final image of the retinal vasculature is obtained by iterative thresholding technique [70]. This algorithm works at a faster rate thus making it an attractive segmentation tool. The iterative thresholding algorithm is based on recursive Taylor expansion of a continuously varying threshold tracking function. Therefore, a binary map of vessels is obtained at the end of this step. Fig.3.5 shows an example image taken from DRIVE database depicting the corresponding binary vessel mask for sub-images.

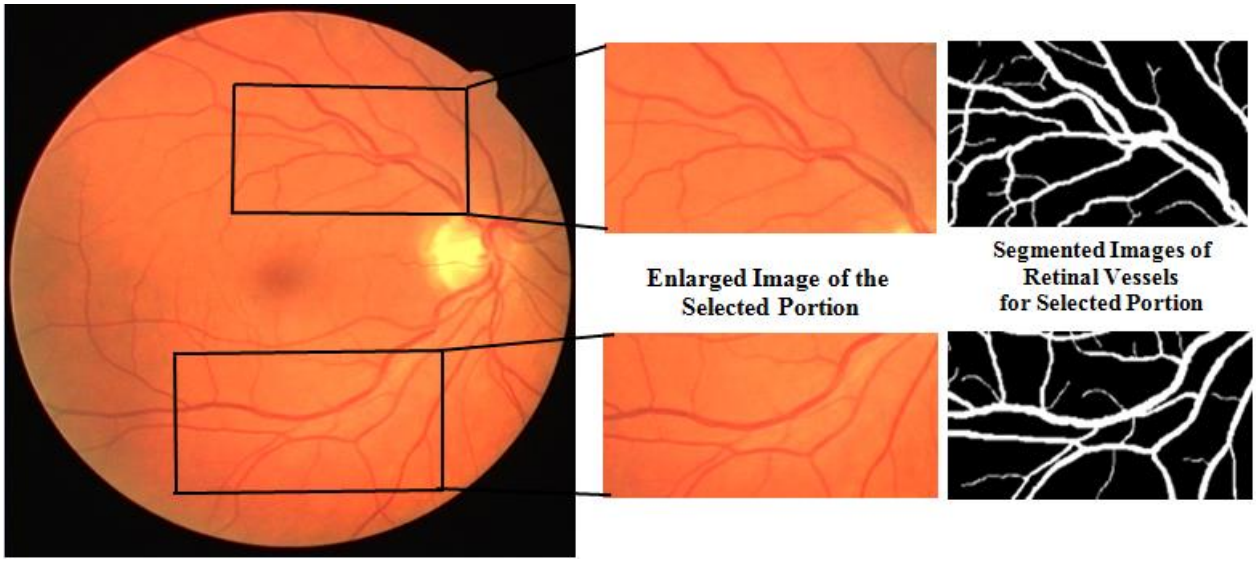

Fig.3.5 Vessel Segmentation: Sub images from the DRIVE database and their corresponding binary vessel mask

(i) Optic disc location and Region of Interest (ROI) selection

The accurate detection of optic disc (OD) location is necessary for determining the ROI required for calculating the AVR, geometrical bifurcation measurements and tortuosity for the diagnosis of hypertensive retinopathy. The optic disc is a large cluster of high intensity pixels. The region of the optic disc is determined by circular Hough transform [71]. The Hough transform is used to identify the locations and orientations of objects which can be parameterized mathematically. The idea behind using the Hough transform is to transform the image into a parametric space which is designed specifically to describe the shape of the desired object. The circular Hough transform is almost identical to the Hough transform for lines, but uses the circular shape for determining the location of optic disc. The parametric form for circle used by the circular Hough transform is given by eq. (3.3)

$$(x - \mathrm{x}_1)^2 + (y - \mathrm{y}_1)^2 = r^2 \qquad (3.3)$$

where $(\mathrm{x}_1, \mathrm{y}_1)$ is the centre of the circle and r denotes the radius of the same circle that passes through (x, y). Fig.3.6 depicts the output obtained by the circular Hough transform for the DRIVE database. Therefore, a circle of optic disc diameter (DD) is drawn after the detection of optic disc location. This circle is assumed to be an outline of the optic disc.

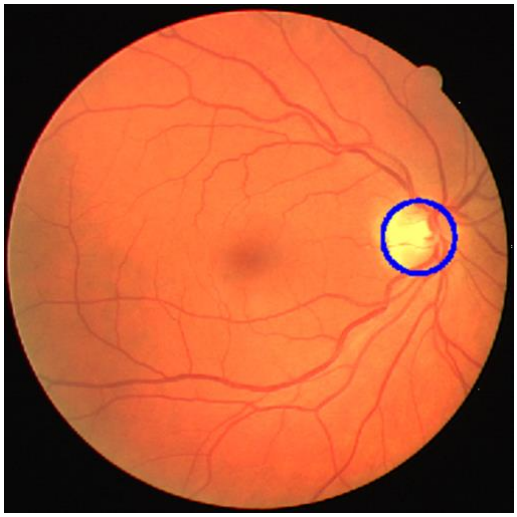

Fig.3.6 Output Image obtained by Hough Transform for the identification of optic disc.

In order to determine AVR, the vessels within the standard circular region A of 1 to 1.5 DD away from the optic disc center is chosen as shown in fig.3.7 [72]. Major arteries and veins present at the linear distance of 1.5 optic disc diameters are the informative vessel segments in an eye. These informative vessel segments range from 6 to 18 per eye while the informative bifurcations in this region range from 8 to 20 per eye [73, 74]. Therefore, the bifurcation features were calculated on a total of 643 bifurcations taken from 40 images of DRIVE and STARE database.

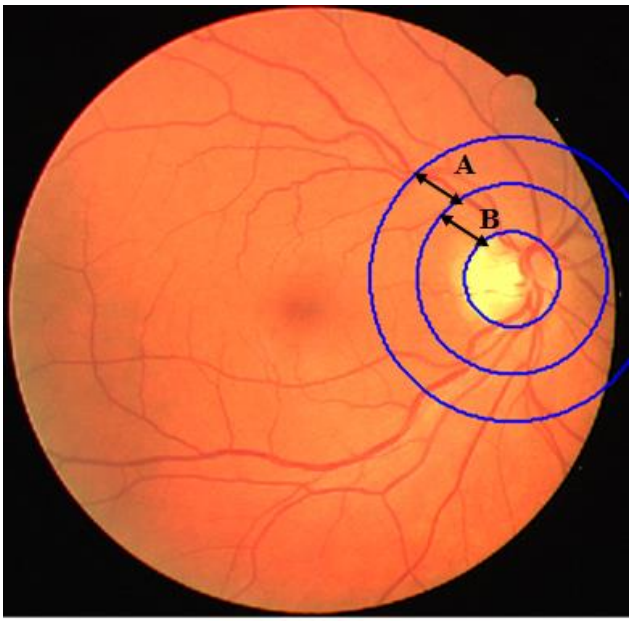

Fig.3.7 Original Image from DRIVE database depicting region A (1 to 1.5) disc diameter and region B depicting (0.5 to 1) disc diameter.

(ii) Artery-Vein (A/V) Discrimination

The diameters of arteries and veins are separately measured to calculate to AVR. Therefore, the retinal vessels must be correctly labeled as arteries and veins inside the region of interest (ROI). The arteries and veins can be discriminated in the basis of visual and geometrical features. Fig.3.8 shows that retinal veins are usually dark and wide while the arteries are bright and thin [75]. Fig.3.9 depicts arteries and veins separately with the help of vessel annotation tool where veins and arteries are represented in green and blue color respectively.

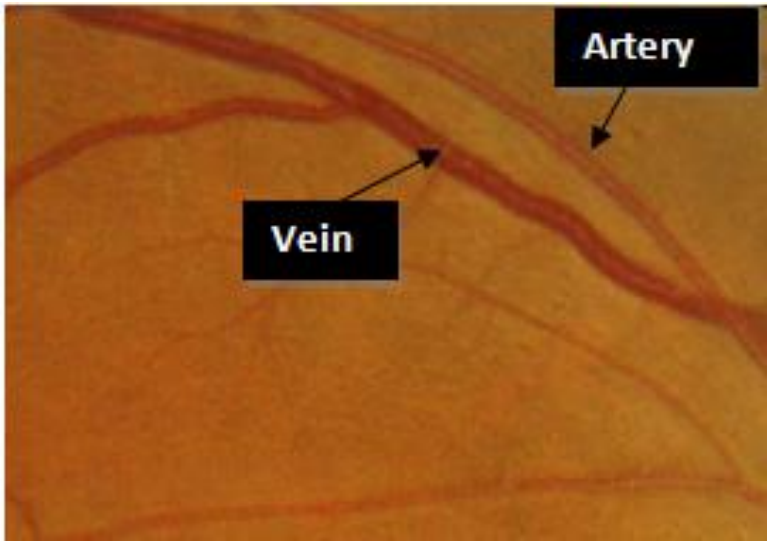

Fig.3.8 Example of an artery and vein

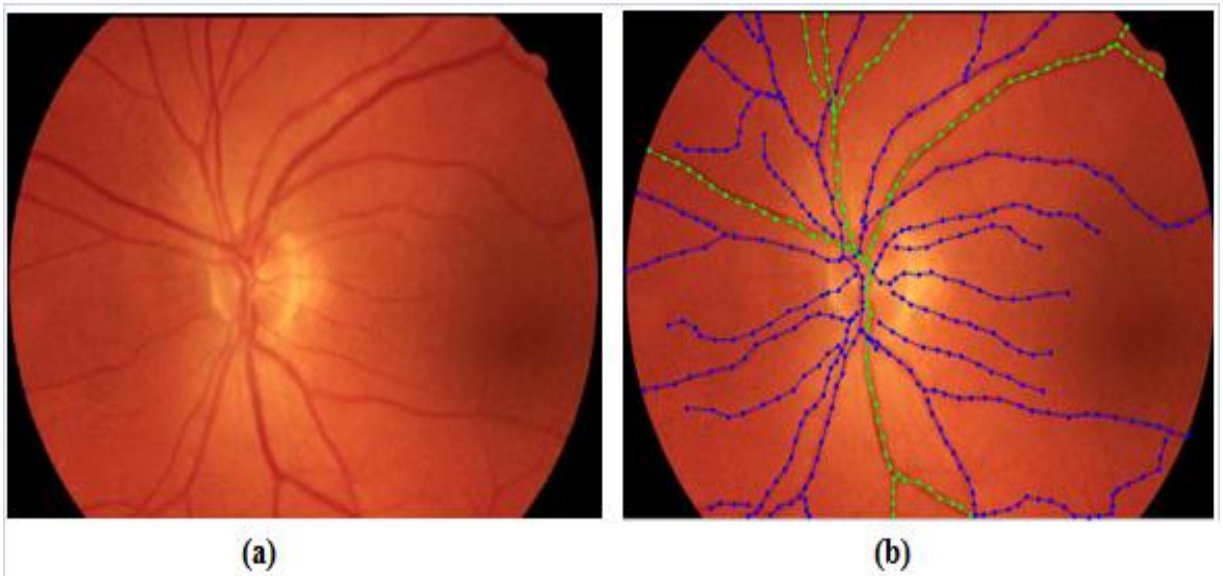

Fig.3.9 Visualization of arteries and veins: (a) Original image from STARE database; (b) Green color indicating veins and blue color indicating arteries.

3.3.2 Performance parameters for vessel segmentation

The results of retinal vessel segmentation are based on pixel classification. Any pixel in the segmented image is classified either as vessel or non-vessel. The classification of pixels is termed as true positive (TP) and true negative (TN) while misclassifications of pixels are termed as false positive (FP), false negative (FN).

True positive (TP) indicates the pixels count that is correctly segmented as a vessel pixel in both segmented image and the gold standard. Similarly, true Negative (TN) indicates the pixels count that is correctly segmented as a non-vessel pixel in both segmented image and the gold standard image. False positive (FP) indicates the pixel count that is marked as a vessel pixel in the segmented image but is actually a non-vessel pixel in the gold standard image. Similarly, false Negative (FN) indicates the pixel count that is segmented as a non-vessel pixel in segmented image but is actually a vessel pixel in the gold standard image.

True Positive Rate (TPR) is the measure of fraction of pixels which are correctly detected as vessel pixels. False Positive Rate (FPR) is the measure of the fraction of pixels which are incorrectly detected as vessel pixels. Specificity (SP) represents the ability to detect the vessel pixels. Specificity (SP) represents the ability to detect non-vessel pixels. Positive predictive value (PPV), also known as the precession rate is the measure of predicted vessel pixels which are true vessel pixels. Accuracy (Acc) is defined as the ratio of the total number of pixels which are correctly classified to the total number of pixels in the image field of view.

3.3.3 Measurements for Detection of Hypertensive Retinopathy

After the proposed segmentation method, a number of measurements on binary retinal vasculature need to be performed; (i) Computation of AVR, (ii) Detection of bifurcation points and (iii) Tortuosity index measurement. All these measurement steps are further discussed below.

(a) Computation of AVR

To get an idea about the vessel width, each vessel in region A of the ROI is divided into small segments. The widths of these segments are calculated by drawing a line perpendicular from the centerline pixel to the edges of the vessels as shown in fig.3.10. This perpendicular from the centerline is drawn in order to minimize the errors which may occur during the width measurement [76]. Vessel width is measured by finding the left and right edges of the vessel in the ROI of vessel map as shown in fig.3.11. Further, euclidean distance is calculated between the left and right edges. The final width of each vessel is calculated by determining the median of width calculated for each small segment.

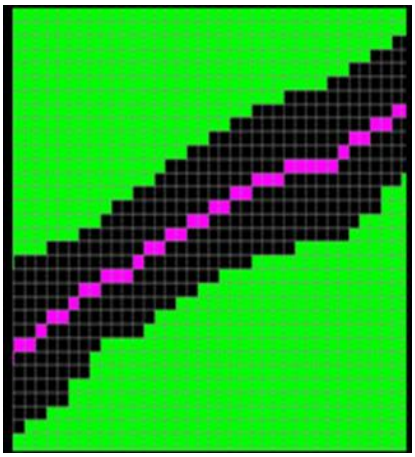

Fig.3.10 Image showing center line pixels (pink color) in the segmented vessel.

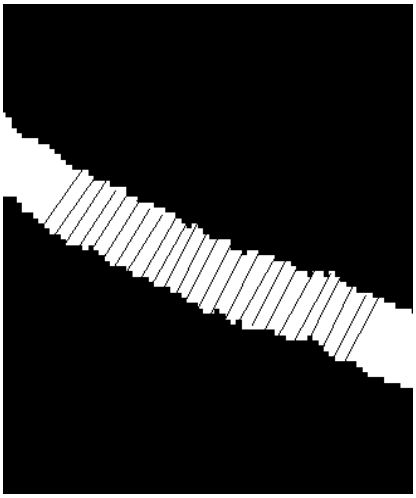

Fig.3.11 Vessel segment of segmented fundus image indicating the vessel width measurement.

The AVR is calculated as the ratio of Central Retinal Arterial Equivalent (CRAE) and Central Retina Venous Equivalent (CRVE) [77]. The CRAE and CRVE are calculated for arterioles and venules respectively. These two measurements are determined by Parr [76], [78] and Hubbard [79] formulas given by:

$$\mathrm{CRAE} = \sqrt{(0.87 * \mathrm{X}^2 + 1.01 * \mathrm{Y}^2 - 0.22 * \mathrm{X} * \mathrm{Y} - 10.73)} \quad (3.4)$$

where Y is the median value in the list of "Arteriole width" and X is the value in the same list exactly before the median Y.

$$\mathrm{CRVE} = \sqrt{(0.72 * \mathrm{X}^2 + 0.91 * \mathrm{Y}^2 + 450.02)} \quad (3.5)$$

where Y is the median value in the list of "Venule width" and X is the value in the list exactly before Y. Arteriolar-to-venular ratio (AVR) is calculated by dividing eq. 3.4 and 3.5

$$\mathrm{AVR} = \frac{\mathrm{CRAE}}{\mathrm{CRVE}} \tag{3.6}$$

The decrease in AVR value provides an indication about the narrowing of blood vessels caused due to hypertensive retinopathy. An AVR value less than 1 indicates that the average arteriolar diameter is narrower than the venular diameter.

(b) Detection of bifurcation points

The prolonged high blood pressure is associated with abnormal changes in the branching geometry of the retinal blood vessels. The bifurcation angle becomes narrower for the hypertensive patients and may be associated with the reduced vascular diameter. Therefore, the detection of bifurcations points has a great significance in the detection of hypertensive retinopathy.

Tree Labeling - After the segmentation of retinal vessel map, they must be labeled. The labeling of vessel tree is done by obtaining its skeleton image [80]. The skeleton image of the vascular tree is obtained by applying a thinning operation on the segmented retinal vasculature. This thinning operation will remove pixels from the vessel boundaries towards the centre but preserves the eight-pixel connectivity [5]. Further, a pruning process is applied to eliminate the false spurs to avoid multiple paths in the eight-connected boundary.

Detecting Significant Points - Bifurcation points, crossing points and end points are the three significant landmarks in the retinal vasculature that must be detected. The skeleton pixels with three neighbors in 3x3 neighborhoods are labeled as bifurcation points. The skeleton pixels with only one neighbor in 3x3 neighborhoods are labeled as end points. Fig.3.12 (a),(b) and (c) depicts the structuring elements used for detecting the bifurcation points while fig.3.12 (d) depicts the structuring element used for detecting the end points. Here '1' defines the set of foreground pixels while '0' defines the set of background pixels. The crossing points appear in the skeleton when two bifurcation points are very close to one another.

1		
0	1	
1	0	1

(a)

	1	
	1	
1	0	1

(b)

	1	
1	1	
		1

(c)

0	1	0
0	0	0

(d)

Fig.3.12 Structuring elements to detect significant points: (a-c) bifurcation points, (d) end points.

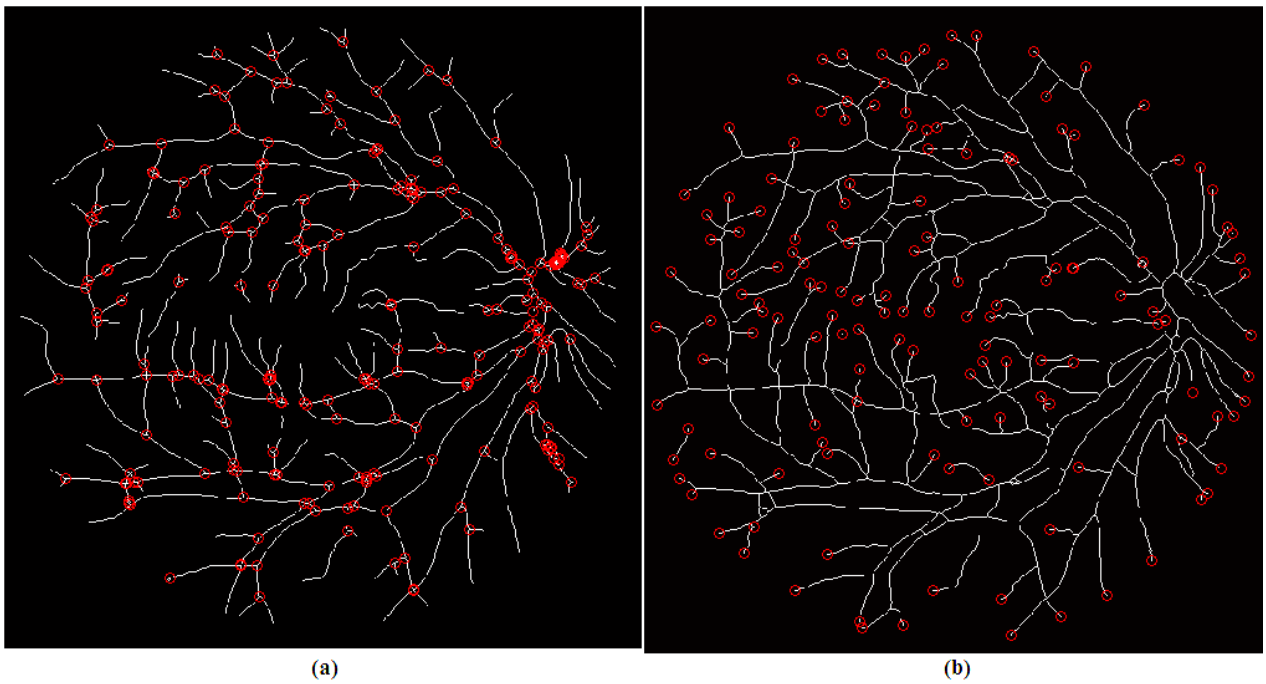

(a) (b)

Fig.3.13 Detected significant points on skeletonized retinal fundus image taken from DRIVE database showing (a) Bifurcation points, (b) End points.

Geometrical Measurements - A number of non-dimensional parameters can be derived from the bifurcations. Murray [80] and Zamir [81] predicted optimum values of these parameters to calculate the minimum power required for the circulation of blood though the bifurcations. The geometrical vessel measurements associated with bifurcations as shown in fig.3.14 are:

1. Angles: Bifurcation angle (θ), angle between parent vessel and larger daughter vessel (θ_1), angle between parent vessel and smaller daughter vessel (θ_2). Bifurcation angle is defined as the angle between two daughter vessels at each bifurcation point $\theta = \theta_1+\theta_2$. The bifurcation angle is calculated along the actual length of the skeleton over a distance of five times the radius for the circular window taken for detecting the bifurcation points. Fig.3.15 depicts the sample images

taken from the test and training sets of the DRIVE database with the corresponding bifurcations selected on which the geometrical measurements are carried out.

2. Vessels diameters (d_0, d_1, d_2): d_0 is the parent vessel diameter while d_1 and d_2 are the diameters of the larger and smaller daughter vessel respectively. These vessel measurements are used to calculate various bifurcation parameters related to parent vessel and the daughter vessel.

Bifurcation Index (α)**:** It is known as degree of asymmetry and is defined as the ratio of diameters of smaller daughter vessel (d_2) to the larger daughter vessel (d_1). $\alpha = d_2 / d_1$ where $0 < \alpha \leq 1$. $\alpha = 1$ indicates that the bifurcations are symmetrical and the vessel diameters are same [52].

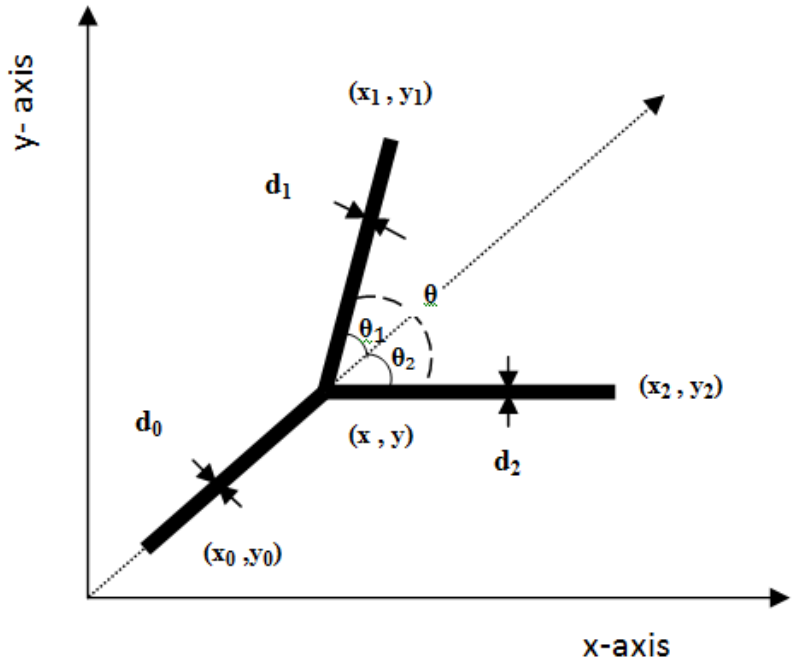

Fig.3.14 Bifurcation measurements such as bifurcation angle between two daughter branches (θ), vessel diameters (d0, d1, d2).

Asymmetry Factor (β)**:** It is also a measure of degree of asymmetry and is defined as the ratio of cross-sectional area of the smaller daughter vessel (d_2) to the larger daughter vessel (d_1). $\beta = d_2^2/d_1^2$ where $0 < \beta \leq 1$. $\beta = 1$ indicates the symmetrical nature of bifurcations.

Ratio of diameters **(σ_1, σ_2):** It is calculated by dividing the diameters of daughter vessels (d_1, d_2) with the parent vessel (d_0) where, $\sigma_1 = d_1/d_0$; $\sigma_2 = d_2/d_0$

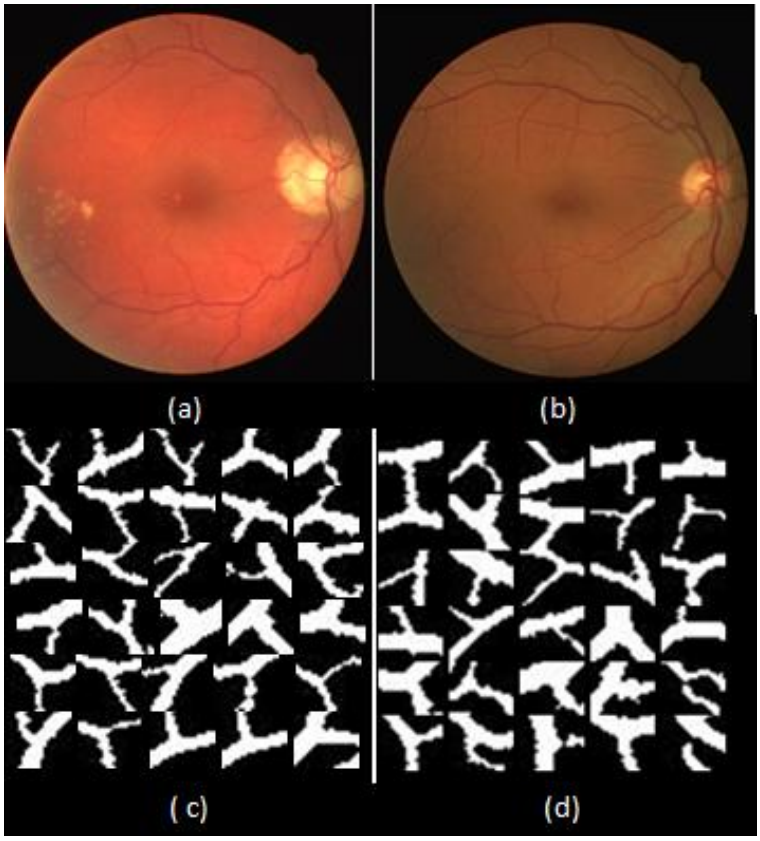

Fig.3.15 (a, b) Original sample image from the test and training datasets respectively taken from the DRIVE database; (c, d) Bifurcation samples taken from the corresponding images.

Area Ratio*(γ)*: It is defined as the sum of cross-sectional areas of the two daughter branches divided by the cross-sectional area of the parent branch. $\gamma = (d_1^2 + d_2^2)/{d_0}^2$

***Junction Exponent* (z):** It provides a relationship between the parent vessel and the daughter vessels ${d_0}^z = {d_1}^z + {d_2}^z$. Murray [80] suggested the optimum value of z to be 3. Although the equation defined below is non-linear therefore the value of z is calculated through the iteration procedure .

(c) Tortuosity index measurement

The vessel tortuosity index is an important factor in determining the severity of hypertensive retinopathy. Therefore, there is a need to assess the tortuosity changes with time. Curvature is a significant attribute in shape analysis and tortuosity evaluation. The tortuosity index is evaluated on a curve C = [x(t), y(t)] on a interval [t_1, t_2] using RET-TORT database from the following methods:

***Ratio of Arc Length over Chord Length* (k):** It is one of the simpler and widely used methods to measure the retinal vessel tortuosity index. It is defined as the ratio between actual length and chord length for the vessel segment given by eq. 3.7, 3.8 and 3.9 [7], [82], [83]. It was first proposed by [83], under the assumption that a non-tortuous retinal vessel is a straight line and the radius of curvature is much larger than the chord. This method compares the length of the curve with respect to the straight distance between its two end points.

The arc length Lx(C) for the curve C is given by,

$$\mathrm{Lx(C)} = \int_{t_1}^{t_2} \sqrt{x'(t)^2 + y'(t)^2}\ \mathrm{dt} \tag{3.7}$$

The cord length Ly(C) of curve C is given by,

$$\mathrm{Ly(C)} = \sqrt{[x(t_2) - x(t_1)]^2 + [y(t_2) - (yt_1)]^2} \tag{3.8}$$

Therefore, $\mathrm{k} = \mathrm{Lx(C)} / \mathrm{Ly(C)}$ (3.9)

***Measures Involving Curvature*:** A number of tortuosity measures involving the use of the integral of absolute curvature (tc) or squared curvature (tsc) have been developed. This is used to measure of the variability of vessel direction.

The curvature v(t) of curve C at t is given by,

$$\mathrm{v(t)} = \frac{x'(t)y''(t) - x''(t)y'(t)}{[y''(t)^2 + x''(t)^2]^{3/2}} \tag{3.10}$$

The absolute curvature tc(C*)* of curve C is,

$$\mathrm{tc(C)} = \int_{t_1}^{t_2} |v(t)|.\,\mathrm{dt} \tag{3.11}$$

The squared curvature tsc(C) of curve C is,

$$\mathrm{tsc(C)} = \int_{t_1}^{t_2} |v(t)^2|.\,\mathrm{dt} \tag{3.12}$$

Table 3.1 describes the various measurements examined in the experiments. These measurements have a minimum value of ‘1’ in case of straight vessel segments and increases positively for the tortuous segments. The more tortuous the vessel is, the larger is its tortuosity index. Any metrics

from τ_1 to τ_7 can be used to quantify tortuosity. The different tortuosity measurements allow us to compare them to determine the relative importance of the tortuosity properties.

Table 3.1. Tortuosity index measures.

Notation	**Tortuosity measure**	**Expression**
τ_1	$\frac{Lx(C)}{Ly(C)}$	$\frac{\text{Arc length}}{\text{Chord length}}$
τ_2	$tc(C)$	Total curvature
τ_3	$tsc(C)$	Total squared curvature
τ_4	$\frac{tc(C)}{Lx(C)}$	$\frac{\text{Total curvature}}{\text{Arc length}}$
τ_5	$\frac{tsc(C)}{Lx(C)}$	$\frac{\text{Total squared curvature}}{\text{Arc length}}$
τ_6	$\frac{tc(C)}{Ly(C)}$	$\frac{\text{Total curvature}}{\text{Chord length}}$
τ_7	$\frac{tsc(C)}{Ly(C)}$	$\frac{\text{Total squared curvature}}{\text{Chord length}}$

CHAPTER-4

EXPERIMENTAL RESULTS

The proposed method is implemented in MATLAB version 8.3.0.532 on a PC with Intel core i3 (1.8 GHZ) processor. The results of proposed segmentation methodology is demonstrated and evaluated on both healthy and pathological retinal fundus images taken from four standard databases, viz., DRIVE, STARE, INSPIRE-AVR, MESSIDOR and RET-TORT [62-66]. The evaluation of the proposed methodology is implemented in four different steps. The first step is the demonstration and evaluation of vessel segmentation results on both DRIVE and STARE databases; the second step is the measurement of AVR on images obtained after applying the proposed segmentation methodology on INSPIRE-AVR and MESSIDOR databases; the third step is the measurements of geometrical properties related to bifurcations on DRIVE and STARE databases and the final step is the measurements related to tortuosity on RET-TORT database. These measurements provide a quantitative summary about the vascular changes in retinal fundus images due to hypertensive retinopathy. The results related to vessel measurements, viz., AVR, bifurcations and tortuosity are validated by comparing them with the available standards in corresponding databases.

4.1 Vessel segmentation results – METHOD 1

The quantitative assessment of the proposed method for the determination of Hypertensive Retinopathy is shown in fig.4.1. The method was successfully able to i) segment the color fundus image and ii) locate the ROI after finding the optic disc center.

Fig.4.1 demonstrates the results of the proposed method on randomly chosen retinal fundus images from the MESSIDOR and INSPIRE-AVR database. Fig.4.1 (a) is the original image taken from the MESSIDOR database and fig.4.1 (b) is the original image taken from the INSPIRE-AVR database. fig.4.1 (c), (d) shows image obtained by dual top-hat transform with respect to that of fig.4.1 (c),(d) respectively. The better contrast image is shown in fig.4.1 (e), (f). The enhanced sample image is then segmented using thresholding technique to get binarized image given by fig.4.1 (g), (h).

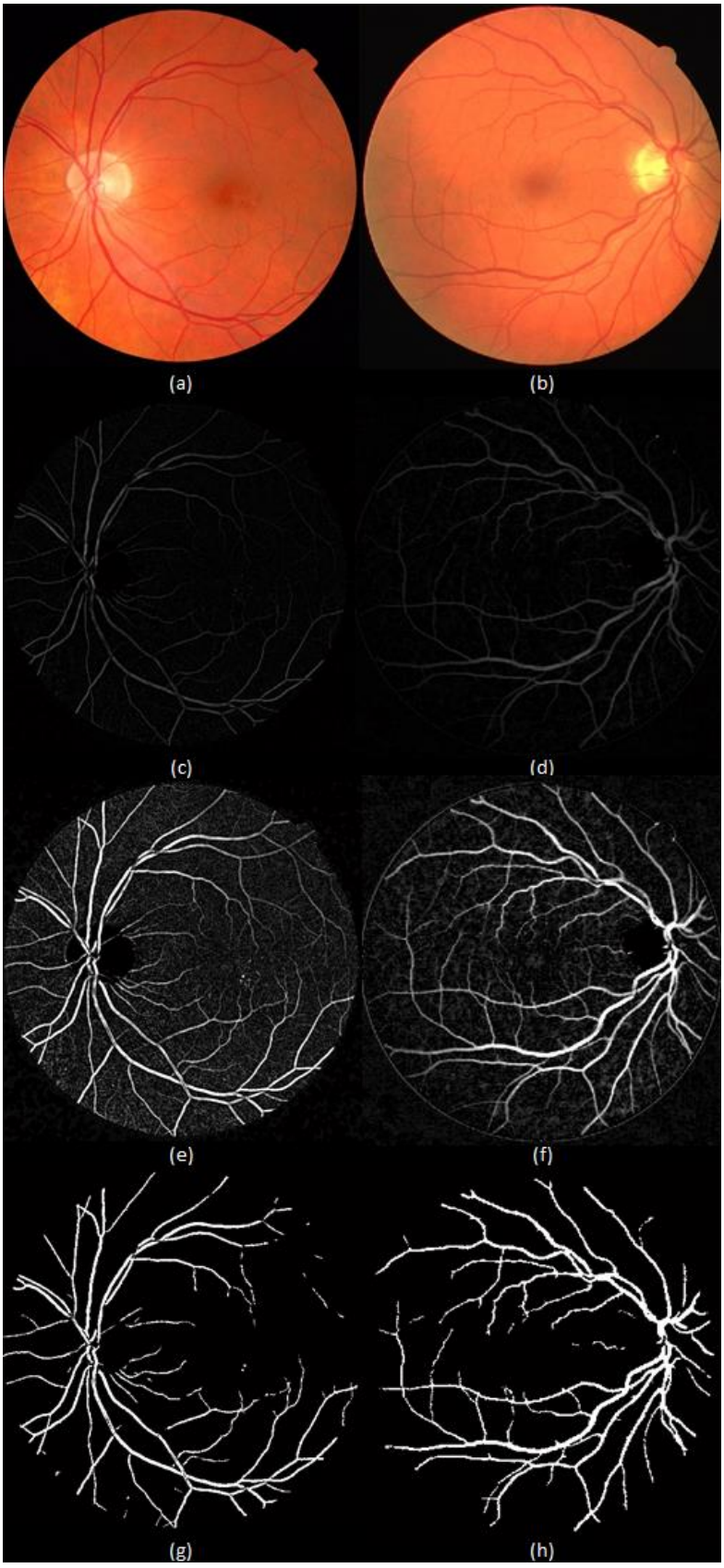

Fig.4.1 Results of processed method: (a-b) original images taken from MESSIDOR, INSPIRE-AVR database respectively, (c-d) output images of dual top-hat transform (e-f) output of enhanced images, (g-h) segmented output images.

The computation of AVR is done by calculating the width of arteries and veins in region A from 1-1.5 DD. The performance of the proposed method on INSPIRE-AVR and MESSIDOR database is shown in table 4.1, table 4.2 respectively. The entire database is summarized in terms of mean, minimum, maximum and standard deviation. Table 4.1 illustrates that mean, minimum, maximum and standard deviation are 0.6374, 0.4968, 0.7898 and 0.0644 respectively for the proposed method with INSPIRE-AVR database. It can be clearly seen from the table 4.1 that the error obtained between the standard reference AVR value and the AVR obtained by the proposed method is very less. Error 1 is the difference between the reference value given by observer 1 and the AVR obtained by the proposed method. Similarly, error 2 is the difference between the reference value given by observer 2 and the AVR obtained by the proposed method

Table 4.2 summarizes the evaluation parameters by showing the mean, minimum, maximum and standard deviation for MESSIDOR database as 0.44629, 0.2026, 0.5992 and 0.0768. The overall performance of the proposed method is compared with the already proposed systems in terms of accuracy as shown in table 4.3. It can be clearly observed that the proposed method has a significant contribution in achieving the accuracy of 97.08% and 97.79% which is higher than the other methods stated in the given table. The AVR of 0.2-0.58 was obtained for the patients suffering from hypertensive retinopathy.

Table 4.1. Overall performance of proposed algorithm for INSPIRE-AVR database.

Sr. No.	Expert1	Expert2	AVR	Diff. 1	Diff. 2
1	0.7	0.71	0.7011	-0.0011	0.0089
2	0.63	0.68	0.6211	0.0089	0.0589
3	0.7	0.65	0.6727	0.0273	-0.0227
4	0.65	0.64	0.6532	-0.0032	-0.0132
5	0.78	0.75	0.7568	0.0232	-0.0068
6	0.65	0.65	0.6471	0.0029	0.0029
7	0.67	0.65	0.6587	0.0113	-0.0087
8	0.64	0.71	0.6888	-0.0488	0.0212
9	0.69	0.76	0.6855	0.0045	0.0745
10	0.56	0.85	0.6859	-0.1259	0.1641
11	0.64	0.74	0.6799	-0.0399	0.0601
12	0.76	0.75	0.776	-0.016	-0.026
13	0.57	0.62	0.5721	-0.0021	0.0479
14	0.62	0.58	0.5732	0.0468	0.0068
15	0.64	0.61	0.6541	-0.0141	-0.0441
16	0.68	0.68	0.6365	0.0435	0.0435
17	0.52	0.45	0.5207	-0.0007	-0.0707
18	0.62	0.63	0.6218	-0.0018	0.0082
19	0.67	0.63	0.643	0.027	-0.013
20	0.71	0.62	0.6622	0.0478	-0.0422

21	0.57	0.58	0.5684	0.0016	0.0116
22	0.72	0.76	0.5634	0.1566	0.1966
23	0.66	0.69	0.6719	-0.0119	0.0181
24	0.65	0.64	0.6534	-0.0034	-0.0134
25	0.56	0.49	0.4968	0.0632	-0.0068
26	0.73	0.61	0.6267	0.1033	-0.0167
27	0.64	0.63	0.6375	0.0025	-0.0075
28	0.63	0.68	0.6327	-0.0027	0.0473
29	0.72	0.7	0.6955	0.0245	0.0045
30	0.59	0.61	0.5955	-0.0055	0.0145
31	0.75	0.75	0.7532	-0.0032	-0.0032
32	0.53	0.61	0.5861	-0.0561	0.0239
33	0.61	0.59	0.5968	0.0132	-0.0068
34	0.65	0.61	0.6146	0.0354	-0.0046
35	0.74	0.64	0.646	0.094	-0.006
36	0.69	0.62	0.6887	0.0013	-0.0687
37	0.82	0.79	0.7898	0.0302	0.0002
38	0.93	0.76	0.6976	0.2324	0.0624
39	0.61	0.64	0.6499	-0.0399	-0.0099
40	0.74	0.62	0.6933	0.0467	-0.0733
Average	0.666	0.6595	0.6492	0.0167	0.0102
Std Dev	0.0804	0.0778	0.0629	0.0576	0.0524
Min	0.52	0.45	0.4968	-0.1259	-0.0733
Max	0.93	0.85	0.7898	0.2324	0.1966

Obs. 1 = Standard reference AVR value assessed by 1st expert.

Obs. 2 = Standard reference AVR value assessed by 2nd expert.

Error 1= (Standard reference AVR value of observer 1) - (AVR value obtained by proposed method)

Error 2= (Standard reference AVR value of observer 2) - (AVR value obtained by proposed method)

SD= Standard Deviation

Min= Minimum AVR value in the corresponding column

Max= Maximum AVR value in the corresponding column

Table 4.2. Overall performance of the proposed algorithm on MESSIDOR database.

Image	**Proposed method output**
1	0.4372
2	0.4803
3	0.5099
4	0.3715
5	0.3026

6	0.4085
7	0.5974
8	0.593
9	0.5992
10	0.446
11	0.506
12	0.4324
13	0.3956
14	0.4548
15	0.4762
16	0.5722
17	0.4738
18	0.3652
19	0.3842
20	0.4857
21	0.4307
22	0.4974
23	0.3253
24	0.3798
25	0.3745
26	0.3491
27	0.3277
28	0.3414
29	0.3975
30	0.4138
31	0.4296
32	0.3914
33	0.4326
34	0.4583
35	0.5869
36	0.5105
37	0.4054
38	0.4505
39	0.4555
40	0.4897
41	0.5542
42	0.5164
43	0.4056
44	0.3452

45	0.3497
46	0.4803
47	0.5206
48	0.5049
49	0.4798
50	0.4052
Mean	**0.44629**
Min	**0.2026**
Max	**0.5992**
SD	**0.07682**

Table 4.3. Performance comparison for Method-1

Author	Dataset (Images)	Accuracy (%)
Ortiz *et al.* [4]	Local (30)	57
Agurto *et al.* [5]	Local (72)	80
Manikis *et al.* [6]	DRIVE	93.71
	STARE	93.18
Khitran *et al.* [7]	VICAVR (58)	96.5
Mirsharif *et al.* [8]	DRIVE	96
Proposed Method	**INSPIRE-AVR (40)**	**97.08, 97.79**
	MESSIDOR (50)	**AVR-0.44629**

4.2 Vessel segmentation results – METHOD 2

Images in Fig.4.2 (a), (b) and (c) are randomly chosen retinal fundus images to demonstrate the segmentation results of proposed method, where Fig. 4.2 (a) and (b) are the original normal images from DRIVE and STARE database while Fig. 4.2 (c) is a pathology image taken from STARE database. The green channel is chosen from the original image and morphological opening is applied on it to obtain a filtered image. Further, a homogenized image is obtained from the filtered image to remove intensity variations. The complement of this homogenized image is taken to obtain a shade corrected image as shown in fig. 4.2 (d), (e) and (f). It can be clearly observed in fig.4.2 (d), (e) and (f) that the global contrast of the image is improved along with the removal of non-uniform illumination effect. The contrast between vessels and background is further enhanced by applying top-hat transform on the shade corrected images. The line structuring element used in the opening operation of top-hat transform is rotated at 22.5°. Lastly, the images with enhanced vessels are obtained by summing up the resultant images after applying top-hat transform at different orientations as shown in fig.4.2 (g), (h) and (i) respectively. Bit-

plane slicing is applied on the enhanced vessel images to get the most significant planes. This is done by combining 7^{th} and 8^{th} bit planes. The final vessel segmented images in fig.4.2 (j), (k) and (l) are obtained using iterative thresholding method on the images obtained by combining 7^{th} and 8^{th} bit planes.

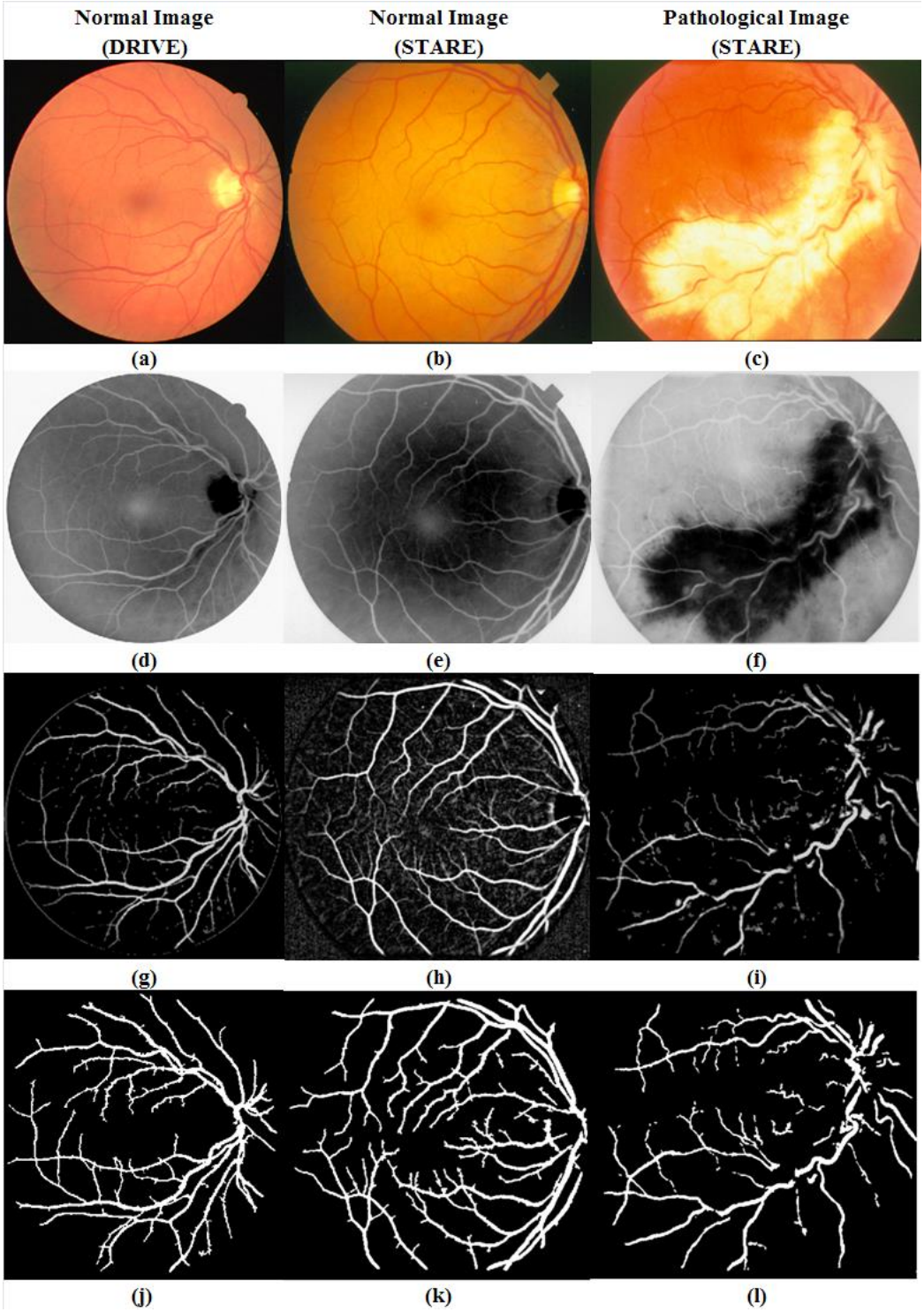

Fig.4.2 Output images obtained by the proposed method; (a-c) Original normal and pathological images from DRIVE and STARE database, (d-f) output image after taking the complement of homogenized image, (g-i) sum of top-hat transform output, (j-l) final segmented images.

The performance of proposed vessel segmentation method is demonstrated on the basis of five medically important statistical measures such as true positive rate, false positive rate, accuracy, specificity, precision using DRIVE and STARE databases. The performance plot of these statistical measures for each image from DRIVE and STARE databases is depicted in fig. 4.3. Table 4.4 summarizes the comparative performance analysis of the proposed vessel segmentation method to that of 2nd human observer which is considered as the ground truth and other state-of-art methods. Table 4.4 clearly illustrates that the average accuracy, sensitivity, specificity and PPV on DRIVE database is 0.9489, 0.7298, 0.9701 and 0.7084 respectively and for the STARE database is 0.9456, 0.7295, 0.9736 and 0.6018 respectively. Table 4.4 clearly indicates that the proposed method outperformed the existing methods in terms of average accuracy, specificity and competitive results in terms of sensitivity.

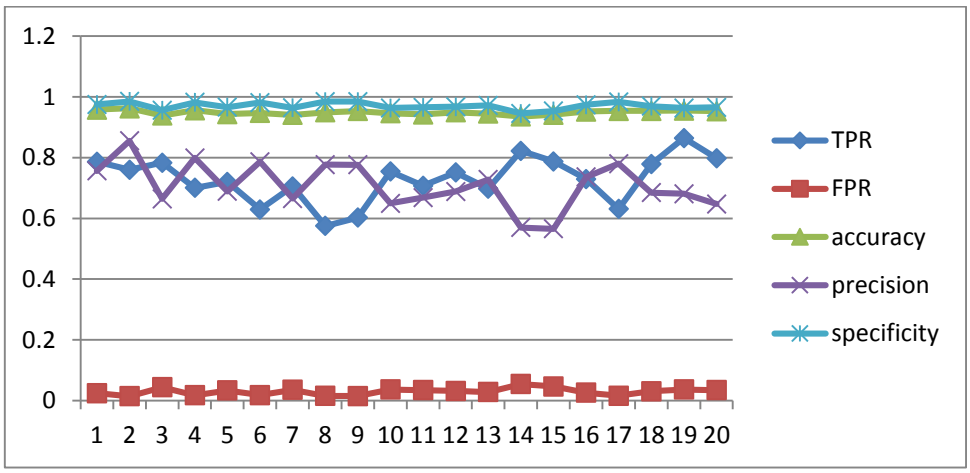

(a) Images from DRIVE database

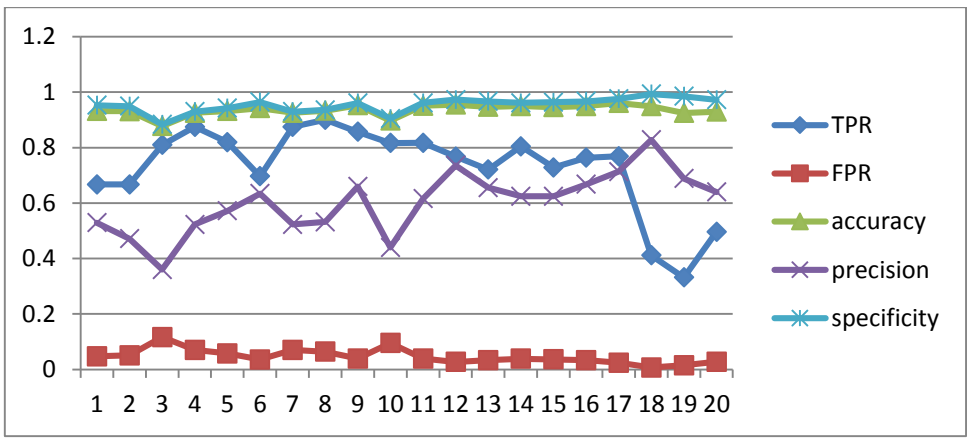

(b) Images from STARE database

Fig.4.3 Performance of proposed segmentation method on images from (a) DRIVE database and (b) STARE database.

Table 4.4. Performance comparison of vessel segmentation methods for DRIVE and STARE databases.

Sr. No.	Methods (DRIVE database)	TPR	FPR	SP	Acc	Stdev(Acc)
1	2nd human observer	0.7763	0.0276	0.9702	0.947	0.0048
2	Chaudhuri et al. [8]	0.3357	-	N.A	0.8773	0.0232
3	Perez et al.[9]	0.785	-	0.949	0.932	-
4	Zana and Klein [11]	0.6971	-	-	0.9377	0.0077
5	Jiang et al.[12]	0.659	-	0.96	0.928	-
6	Mendonca and Campilho [15]	0.7344	-	0.9764	0.9452	-
7	Perez et al. [17]	0.7246	-	0.9655	0.9344	-
8	Perez et al. [18]	0.66	-	0.9612	0.922	-
9	Espona et al. [20]	0.6634	-	0.9682	0.9316	-
10	Al-Diri et al. [27]	0.7282	-	0.9551		-
11	Rossant et al. [33]	0.7031	-	0.9701	0.9433	-
12	Fraz et al. [34]	0.7224	-	0.9711	0.9469	-
13	Wang et al. [36]	-	-		0.9461	-
14	Chakraborti et al. [38]	0.7205	-	0.9579	0.937	-
15	**Proposed methodology**	**0.7298**	**0.0298**	**0.9701**	**0.9489**	**0.0071**
Sr. No.	**Methods (STARE database)**	**TPR**	**FPR**	**SP**	**Acc**	**Stdev(Acc)**
1	2nd human observer	0.8951	0.06157	0.9384	0.9348	-
2	Hoover et al. [10]	0.6751	-	0.9567	0.9267	-
3	Vermeer et al. [13]	-	-	-	0.9287	-
4	Mendonca and Campilho [15]	0.6996	-	0.973	0.944	-
5	Perez et al. [17]	0.7506	-	0.9569	0.941	-
6	Perez et al. [18]	0.779	-	0.9409	0.924	-
7	Al-Diri et al. [27]	0.7521	-	0.9681	-	-
8	Gonzalez et al. [37]	0.7887	0.0367	-	0.9441	-
9	Chakraborti et al. [38]	0.6786	-	0.9586	0.9379	-
10	**Proposed Method**	**0.7295**	**0.0463**	**0.9736**	**0.9456**	**0.15391**

* TPR - True positive rate, FPR - False positive rate, SP - Specificity, Acc - Accuracy, Stdev (Acc) - Standard Deviation of accuracy

4.3 Quantitative measurements to detect Hypertensive Retinopathy

The evaluation of the proposed segmentation method for detection of hypertensive retinopathy is performed by calculating parameters like AVR, bifurcation parameters and tortuosity on segmented vasculature images. These measurements are validated by standard results available with the respective databases.

4.3.1 Arterio-to-venular ratio (AVR) Results

The values of AVR are computed by calculating the ratio of width of arteries and veins on segmented retinal images inside the region A (1-1.5 DD) as shown in fig.3.7. Table 4.5 illustrates the results on 40 images of INSPIRE-AVR database which is summarized in terms of average, minimum, maximum and standard deviation. It can be seen clearly from table 4.5 that diff. 1 and diff. 2 are the difference values of AVR measured on segmented images by the proposed method to that of standard references provided by expert1 and expert 2 respectively. An average difference of 1.67% and 1.02% was calculated between the measured AVR and expert 1 and 2 respectively. Also, it can be clearly seen from the table 4.5 that the AVR values calculated on segmented images are in clear agreement to that of the expert opinions. The average accuracy of AVR calculated by the proposed method was found to be 97.44% and 98.43% with respect to expert 1 and expert 2.

The agreement between the proposed method and the reference standard can be demonstrated in terms of Bland-Altman statistical plots illustrated in fig.4.4. It is also known as difference plot that provides limits of agreement between two methods. The x-axis represents the averages values while the y-axis represents the difference values between the calculated AVR and the reference standard. The horizontal red dotted lines represent the limits of agreement. It is defined as mean difference ± 1.96 standard deviation of the difference. The blue horizontal lines bounding the limits of agreement represents the confidence interval bands for the limits of agreement. The bolded blue line near the centre of Bland-Altman plot represents the line of equality which is defined as the mean difference between AVR measurements. If the line of equality is not in within the interval then there is a significant difference between two measurements. The Bland–Altman plots show that both the proposed method and the experts view have no substantial bias because the mean difference between both AVR measurements is very close to 0.

Table 4.5. AVR values obtained for each image of INSPIRE-AVR database.

Sr. No.	AVR_{E1}	AVR_{E2}	AVR_{PSM}	Diff. 1	Diff. 2
1	0.7	0.71	0.7011	-0.0011	0.0089
2	0.63	0.68	0.6211	0.0089	0.0589
3	0.7	0.65	0.6727	0.0273	-0.0227
4	0.65	0.64	0.6532	-0.0032	-0.0132
5	0.78	0.75	0.7568	0.0232	-0.0068
6	0.65	0.65	0.6471	0.0029	0.0029
7	0.67	0.65	0.6587	0.0113	-0.0087
8	0.64	0.71	0.6888	-0.0488	0.0212
9	0.69	0.76	0.6855	0.0045	0.0745
10	0.56	0.85	0.6859	-0.1259	0.1641

11	0.64	0.74	0.6799	-0.0399	0.0601
12	0.76	0.75	0.776	-0.016	-0.026
13	0.57	0.62	0.5721	-0.0021	0.0479
14	0.62	0.58	0.5732	0.0468	0.0068
15	0.64	0.61	0.6541	-0.0141	-0.0441
16	0.68	0.68	0.6365	0.0435	0.0435
17	0.52	0.45	0.5207	-0.0007	-0.0707
18	0.62	0.63	0.6218	-0.0018	0.0082
19	0.67	0.63	0.643	0.027	-0.013
20	0.71	0.62	0.6622	0.0478	-0.0422
21	0.57	0.58	0.5684	0.0016	0.0116
22	0.72	0.76	0.5634	0.1566	0.1966
23	0.66	0.69	0.6719	-0.0119	0.0181
24	0.65	0.64	0.6534	-0.0034	-0.0134
25	0.56	0.49	0.4968	0.0632	-0.0068
26	0.73	0.61	0.6267	0.1033	-0.0167
27	0.64	0.63	0.6375	0.0025	-0.0075
28	0.63	0.68	0.6327	-0.0027	0.0473
29	0.72	0.7	0.6955	0.0245	0.0045
30	0.59	0.61	0.5955	-0.0055	0.0145
31	0.75	0.75	0.7532	-0.0032	-0.0032
32	0.53	0.61	0.5861	-0.0561	0.0239
33	0.61	0.59	0.5968	0.0132	-0.0068
34	0.65	0.61	0.6146	0.0354	-0.0046
35	0.74	0.64	0.646	0.094	-0.006
36	0.69	0.62	0.6887	0.0013	-0.0687
37	0.82	0.79	0.7898	0.0302	0.0002
38	0.93	0.76	0.6976	0.2324	0.0624
39	0.61	0.64	0.6499	-0.0399	-0.0099
40	0.74	0.62	0.6933	0.0467	-0.0733
Average	0.666	0.6595	0.6492	0.0167	0.0102
Std Dev	0.0804	0.0778	0.0629	0.0576	0.0524
Min	0.52	0.45	0.4968	-0.1259	-0.0733
Max	0.93	0.85	0.7898	0.2324	0.1966

where AVR_{E1} is the AVR value provided by expert 1, AVR_{E2} is the AVR value provided by expert 2, AVR_{PSM} is the AVR value obtained by the proposed segmentation method, Diff. 1 is the error value between obtained AVR value and expert 1 and Diff. 2 is the error value between obtained AVR value and expert 2.

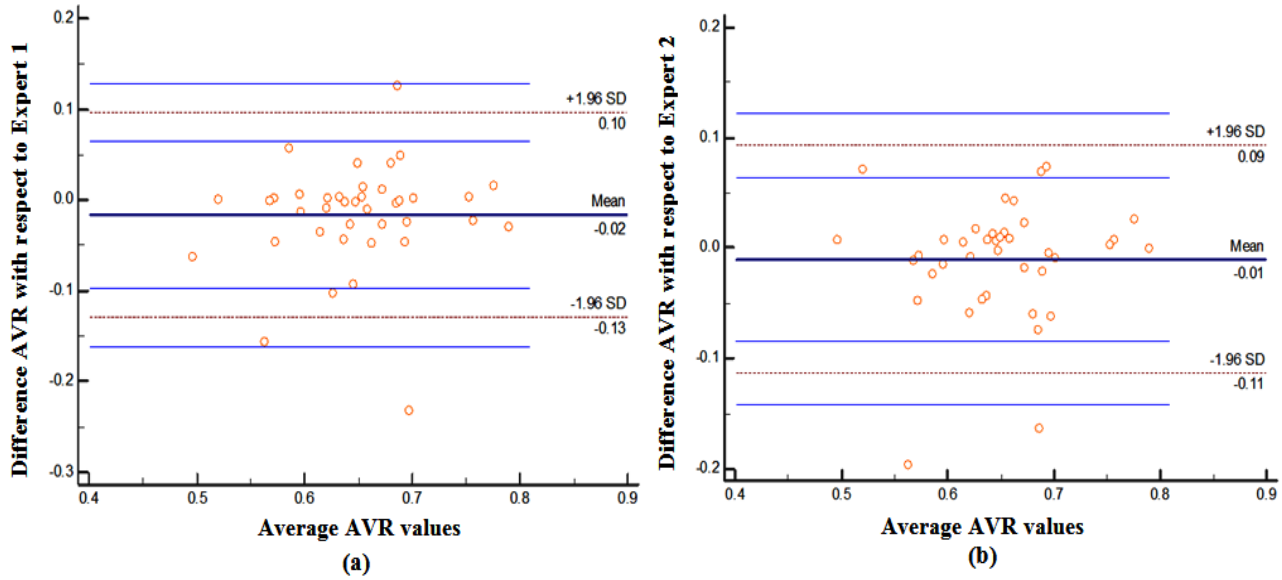

Fig.4.4 Bland–Altman plots of the agreement between the AVR obtained by the proposed method and the reference standard; (a) agreement between the proposed method and Expert 1, (b) agreement between the proposed method and Expert 2. The blue lines represent the 95% limits of agreement and the bolded blue line represents the mean difference between AVR measurements.

4.3.2 Geometrical Measurement results for bifurcation points

The quantitative assessment of the proposed method is done by measuring geometrical properties on 643 bifurcations taken from 40 images of DRIVE and STARE database. These geometrical measurements are summarized in table 10 in terms of minimum, maximum, mean, median, standard deviation and variance for DRIVE and STARE database. The measurements are presented in terms of θ, d_0, d_1, d_2, α, β, σ_1, σ_2, γ. Branching angles (θ) have been reported to be more acute in the patients suffering from hypertensive retinopathy. Zamir [84] suggested that the optimal value of bifurcation angle (θ) is 75°<θ<102° for normal retina.

In the present work, 73.61% of bifurcation angles fall into the normal range for DRIVE database. The bifurcation angle in case of abnormal images were found in the range of 29.04°<θ<74°. In case of STARE database, 61.68% bifurcation angles were found to be in the normal range while the bifurcation angles for the abnormal retinal images were found to be 39.87°<θ<74°. Theoretically, the relationship of vessel diameters is in the form of $d_0 \geq d_1 \geq d_2$. However, the diameter of retinal blood vessels may decrease with the increase in hypertension. In 6.2% cases, it was examined that $d_2 > d_1$.

The parameters like α, β, σ_1, σ_2, γ which depends on the vessel diameters should be less than one but it may exceed sometimes. This may occur due to pathological changes, natural variations or due to presence of curvature. The asymmetry factors α, β, σ_1 and σ_2 indicates relationship

between diameters of the parent branch with respect to the daughter branches. The bifurcation is symmetrical if the asymmetry factors lie in between 0 and 1. It can be clearly seen from table 4.6 that the mean values for these parameters are very close to optimal value 1 for both DRIVE and STARE databases. The area ratio (γ) provides a relationship between the diameters of all three branch segments. The optimal value of γ for a symmetrical bifurcation lies between 1 and 1.4. Table 4.6 illustrates that a mean value of 1.0594 is obtained for the area ratio with a standard deviation of 0.2837 in case of DRIVE database. While, in case of STARE database a mean value of 1.8481 is obtained with a standard deviation of 1.0589.

Further, Fig.4.5 represents the above mentioned results in terms of overall performance of the proposed method with 643 bifurcation points in terms of box plots. Fig.4.5 (a) and (b) illustrates the bifurcation angle representing the normal and abnormal cases for DRIVE and STARE database respectively. Also, Fig.4.5 (c) and (d) presents the relationship between parent (d_0) and both daughter branches (d_1), (d_2) in terms of diameter.

Table 4.6. Geometrical measurements on bifurcation points using DRIVE and STARE databases.

DRIVE	**θ**	**d_0**	**d_1**	**d_2**	**α**	**β**	**σ_1**	**σ_2**	**γ**
MIN:	29.0412	2	1.59	1.06	0.2936	0.0862	0.3957	0.2542	0.2923
MAX:	157.1114	10.3	7.49	6.51	1.8432	1.3976	0.996	0.984	1.8507
MEAN:	82.503	4.9504	3.9925	3.0108	0.7669	0.615	0.8081	0.6134	1.0594
MEDIAN:	86.1215	4.94	3.94	3	0.7773	0.6043	0.8141	0.6122	1.028
STD DEV.	26.2662	1.2886	1.1564	0.9609	0.1638	0.2751	0.1131	0.132	0.2837
VARIANCE:	289.9157	1.6606	1.3373	0.9234	0.0268	0.0756	0.0128	0.0174	0.0804
STARE	**θ**	**d_0**	**d_1**	**d_2**	**α**	**β**	**σ_1**	**σ_2**	**γ**
MIN:	39.8713	1.88	0.94	0.81	0.2596	0.0674	0.4563	0.206	0.2506
MAX:	179.0756	7.97	7	5	1.9648	1.2693	0.998	0.9539	1.1568
MEAN:	82.3917	4.3188	3.5934	2.3650	0.668	0.484	0.8306	0.5487	1.8481
MEDIAN:	109.2546	4.085	3.68	2.06	0.6852	0.4695	0.8507	0.5243	1.0299
STD DEV.	23.6160	1.3348	1.2323	1.0144	0.1948	0.2614	0.1296	0.1641	1.0589
VARIANCE:	257.7180	1.7817	1.5187	1.0290	0.0379	0.0683	0.0168	0.0269	0.1027

where θ = bifurcation angle, d_0 = parent vessel diameter, d_1= larger daughter diameter, d_2 = smaller daughter diameter, α = Bifurcation Index, β = Asymmetry Factor,(σ_1 , σ_2)= Ratio of diameters, γ = Area Ratio

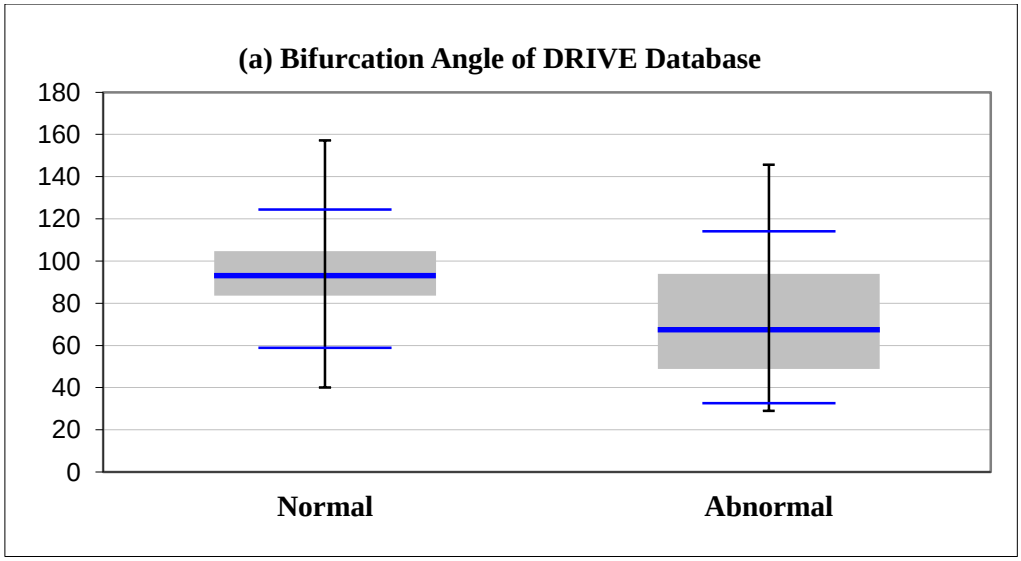
(a) Bifurcation Angle of DRIVE Database
180
160
140
120
100
80
60
40
20
0
Normal
Abnormal

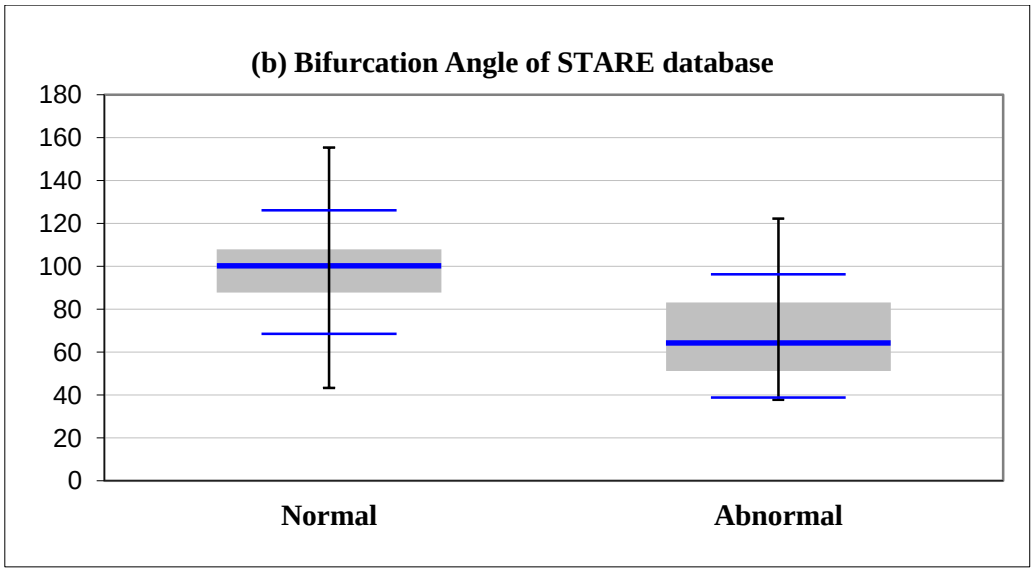
(b) Bifurcation Angle of STARE database
180
160
140
120
100
80
60
40
20
0
Normal
Abnormal

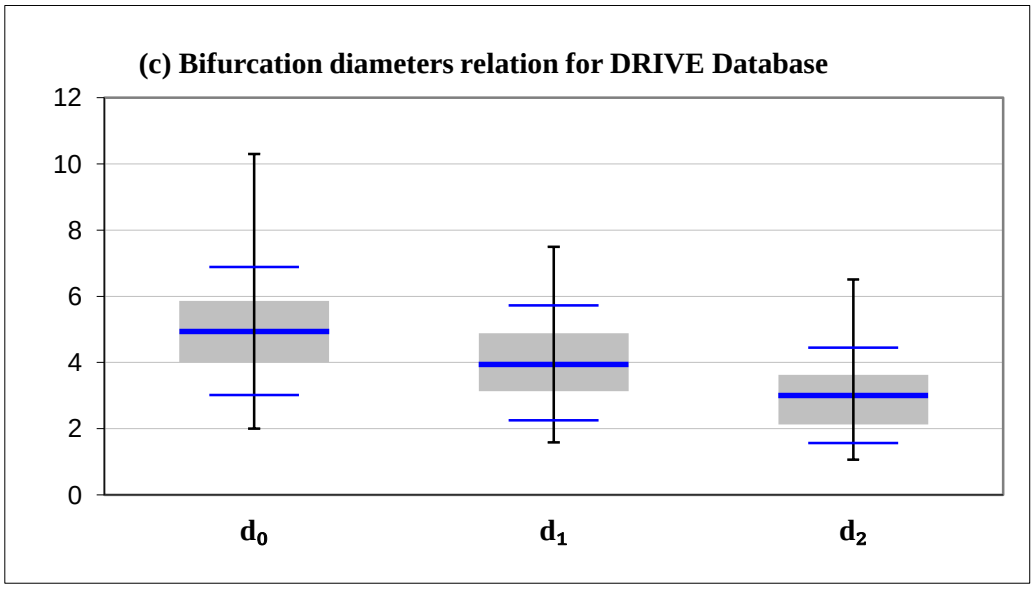
(c) Bifurcation diameters relation for DRIVE Database
12
10
8
6
4
2
0
d0
d1
d2

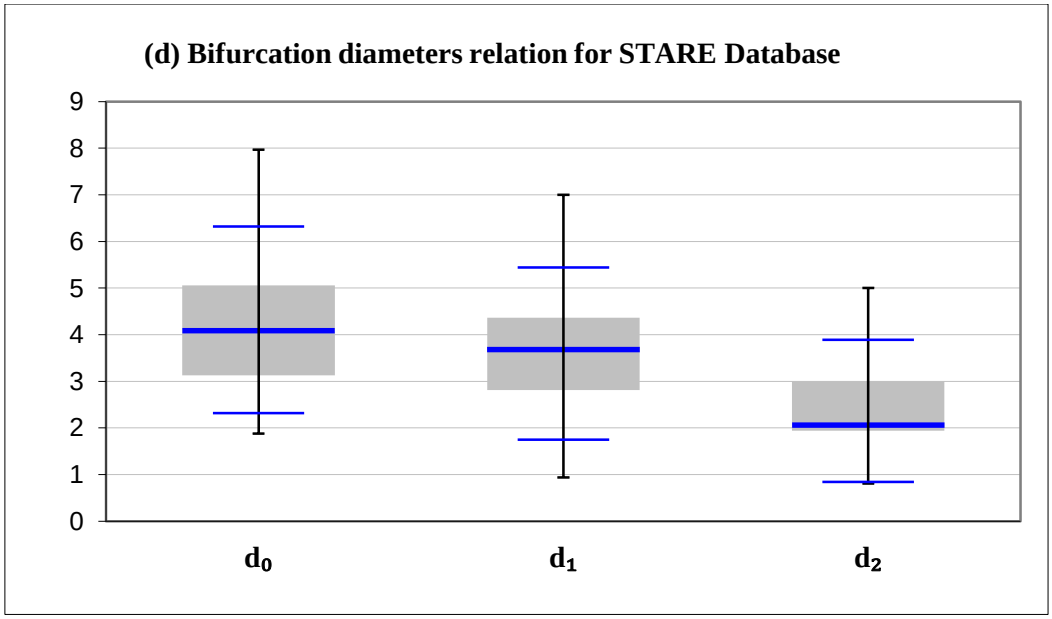

Fig.4.5 Summary of the overall performance on 643 bifurcations for DRIVE and STARE databases where d_0, d_1, d_2 represents the vessel diameter of parent, large daughter and small daughter branch respectively.

4.3.3 Tortuosity Measurement Results

The tortuosity measurements τ_1 to τ_7 are carried on a publicly available database RET-TORT containing 60 vessel segments. Since, the RET-TORT database contains ranking for the tortuous vessels provided by experts, therefore spearman correlation coefficient **(ρ)** is considered as a performance measure. It provides a measure of closeness of ranking between the tortuosity parameters illustrated in table 4.7 with respect to the ranking provided by the expert. The spearman correlation coefficient varies between -1 to 1. Here, a negative represents the negative correlation and positive value represents positive correlation. Table 4.7 shows the median values of the spearman correlation coefficient for arteries and veins separately using various tortuosity measures discussed. It can be clearly observed that the introduction of curvature and amplitude study has improved the correlation value at a significant rate. Table 4.7 indicates a strong positive correlation between the ophthalmologist's ranking and the measured ranking. These measurements can be used to give a comparison between the structural properties used to analyze the tortuosity index. The proximity of the measurement results, obtained after the implementation of proposed segmentation methodology to the standard values suggests the candidacy of the proposed segmentation methodology in the detection and grading of hypertensive retinopathy if this method is implemented in the CAD system.

Table 4.7. Median Values of the Spearman Correlation Coefficient (ρ) for the Tortuosity Measure on 30 Arteries and Veins from RET-TORT database.

R_A	R_V	$R_{A\tau1}$	$R_{V\tau1}$	$R_{A\tau2}$	$R_{V\tau2}$	$R_{A\tau3}$	$R_{V\tau3}$	$R_{A\tau4}$	$R_{V\tau4}$	$R_{A\tau5}$	$R_{V\tau5}$	$R_{A\tau6}$	$R_{V\tau6}$	$R_{A\tau7}$	$R_{V\tau7}$
13	25	10	25	13	25	13	25	13	25	13	25	13	25	13	23
12	3	11	3	12	3	12	3	12	3	12	3	12	3	12	3
30	16	29	16	30	16	30	16	30	16	30	16	30	16	30	16
26	2	25	2	26	1	26	2	26	2	26	2	26	2	26	2
24	8	21	8	24	8	24	8	24	8	24	8	24	8	24	8
29	12	27	12	26	12	29	12	29	12	29	12	29	12	29	12
28	15	26	15	28	15	28	13	28	15	28	15	28	15	28	15
19	24	17	22	19	25	16	24	19	24	19	24	19	24	19	24
17	18	14	16	17	18	17	18	17	18	17	18	17	18	17	18
18	28	18	28	15	28	18	28	18	23	14	28	18	28	18	28
23	29	23	29	23	24	23	29	21	29	23	29	23	29	23	26
4	6	4	6	4	6	4	6	4	6	4	6	4	6	4	6
9	30	9	29	9	30	9	28	9	30	9	30	9	30	9	29
2	10	2	8	2	10	2	10	2	10	2	10	2	10	2	10
8	4	8	4	8	4	8	4	8	4	8	4	8	4	8	4
15	1	15	1	17	2	15	1	15	1	15	1	15	1	15	1
7	19	7	19	7	19	7	19	7	19	7	19	7	19	7	19
10	23	10	23	10	23	10	23	10	21	10	21	10	23	10	23
14	22	14	22	14	22	14	22	14	22	16	22	14	22	14	22
22	13	22	13	22	13	22	15	22	13	22	13	22	13	22	13
27	9	27	9	27	9	27	9	22	9	27	9	27	9	22	9
6	17	6	17	6	17	6	17	6	17	6	17	6	17	6	17
20	21	20	21	18	21	20	21	20	21	19	21	20	21	20	21
3	11	3	11	3	11	3	11	3	11	3	11	3	11	3	11
11	20	11	20	11	20	11	20	11	20	11	20	11	20	11	18
5	14	5	14	5	14	5	14	5	14	5	14	5	14	5	14
1	7	1	7	1	7	1	7	1	7	1	7	1	7	1	7
16	27	16	25	16	27	14	24	16	26	16	25	16	26	16	27
21	27	21	27	21	27	21	27	20	27	21	27	21	22	21	27
25	26	25	26	25	26	25	26	25	23	25	26	25	26	25	26
Median ρ		**0.792**	**0.658**	**0.92**	**0.822**	**0.919**	**0.919**	**0.918**	**0.814**	**0.913**	**0.773**	**0.937**	**0.804**	**0.928**	**0.842**

CHAPTER-5

DISCUSSION

An automated segmentation method to identify blood vessels and calculate features like arteriolar to venular ratio, bifurcations and tortuosity in color fundus images for the detection of hypertensive retinopathy has been presented in this paper. The proposed method has been tested on two established publicly available databases DRIVE and STARE for their segmentation results. The AVR measurement was carried out on a standard database INSPIRE-AVR, while the tortousity was estimated on a new public database RET-TORT. The experimental results prove that the performance achieved with the proposed method are quite comparable, and in some cases, even exceed the recently published results, and approximate to the performance of human observers. It is noteworthy that the average values for true positives (sensitivity), false negative, specificity, PPV and accuracy which assess the agreement of the individual pixel classification with the ground truth vessel and non vessel classes, respectively, are, in most cases, higher than those reported by other authors.

The proposed vessel segmentation method employs a combination of different image processing techniques which encompasses the use of the multidirectional top-hat transform having different orientations for the vessel enhancement along with the application of morphological bit plane slicing technique. The final retinal vasculature is obtained by segmenting the vessels using iterative thresholding technique. In case of DRIVE database, the average accuracy, specificity and PPV of the proposed method is 0.9489, 0.9701 and 0.7084 with a true positive rate and false positive rate of 0.7298 and 0.0298, respectively. The proposed method is better in terms of average accuracy than second observer and the work of other authors like Chaudhuri et al. [8], Perez et al. [9], Zana and Klein [11], Jiang et al. [12], Mendonca and Campilho [15], Perez et al. [17,18], Espona et al. [20], Anzalone et al. [22], Rossant et al. [33], Fraz et al. [34], Wang et al. [36] and Chakraborti et al. [38]. The proposed method has achieved higher true positive rate than Chaudhuri et al. [8], Zana and Klein [11], Jiang et al.[12], Perez et al. [17,18], Espona et al. [20], Al-Diri et al. [27], Rossant et al. [33], Fraz et al. [34], and Chakraborti et al. [38]. For the STARE dataset, the average accuracy, specificity produced by the proposed method is 0.9456, 0.9736 with a true positive rate and false positive rate of 0.7295 and 0.0463 respectively. There is an improvement in terms of accuracy and true positive rate in the results of the proposed method as compared to previous work of Hoover et al. [10], Vermeer et al. [13], Mendonca and Campilho

[15], Perez et al. [17,18], Al-Diri et al. [27], Gonzalez et al. [37] and Chakraborti et al. [38]. It can be easily observed that the proposed method achieves very good accuracy, sensitivity and specificity than all the state-of-art methods.

The AVR values estimated by the semi-automatic procedure shows that the mean AVR and standard deviation for the INSPIRE-AVR database is 0.6492 and 0.0629 with the minimum and maximum value of 0.4968 and 0.7898 respectively. An average error of 0.0167 and 0.0102 was calculated between proposed method and experts 1, 2 respectively. Therefore, the average AVR measured and standard reference are very close to one another. The measurement of AVR on proposed segmentation method achieved a high accuracy of 97.44% with respect to expert 1 and 98.43% with respect to expert 2. Also, a detailed experimental study has been provided for the bifurcation points on a large database of 643 bifurcations from the DRIVE and STARE databases. A larger database is essential to provide a generalized result related to changes in the vessel geometry due to hypertensive retinopathy. It was observed that the bifurcation angle become acute in the abnormal cases and varies at an angle of $29.04° < \theta < 74°$ for DRIVE database while $39.87° < \theta < 74°$ for STARE database. The arteriolar narrowing also plays a significant role in the branching geometry for the hypertensive patients. The diameter of the daughter vessel branch is observed to be higher than the parent branch in the abnormal retinal cases. The experimental results for calculating tortuosity index shows that the study of curvatures presents in the torturous vessel plays a significant role for the patients suffering with hypertension. The correlation with respect to expert opinion has been discussed for various tortuosity measurement methods to show the most significant property affecting the tortuosity of the retinal vessel.

CHAPTER-6

CONCLUSION AND FUTURE SCOPE

The various diagnostically important performance measures defining the detection of hypertensive retinopathy has been successfully done by the proposed automated blood vessel segmentation method. The segmented blood vasculature achieves a very high accuracy and therefore allows accurate quantitative measurement of arteriolar-to-venular ratio, bifurcation angles and toruosity to determine the abnormal changes due to hypertension. Finally, it can be emphasized that the proposed method may be used potentially to aid ophthalmologists in early detection of hypertensive retinopathy and effective planning can be done to control the progression of the disease.

In future work, a fully automated measurement of bifurcations and tortuosity can play an important part of retinal image analysis tools. Various tortuosity tools have been developed based on curvature so far. Another important direction to extend the work is to take into account the vessel diameter as it also plays an important role in computation of tortuosity. This is because wide vessels in general have thick walls, and hence even a small bend in a thick vessel may characterize an abnormal tortuous vessel, while more bend were necessary to characterize tortuosity of thin vessels.

REFERENCES

[1] A. Chobanian, "Control of Hypertension — An Important National Priority", New England Journal of Medicine, vol. 345, no.7, pp. 534-535, 2001.

[2] P. Kearney, M. Whelton, K. Reynolds, P. Muntner, P. Whelton and J. He, "Global burden of hypertension: analysis of worldwide data", The Lancet, vol. 365, no. 9455, pp. 217-223, 2005.

[3] N. Keith, H. Wagener and N. Barker, "Some Different Types Of Essential Hypertension", The American Journal of the Medical Sciences, vol. 197, no. 3, pp. 332-343, 1939.

[4] G. Azzopardi and N. Petkov, "Automatic detection of vascular bifurcations in segmented retinal images using trainable COSFIRE filters", Pattern Recognition Letters, vol. 34, no. 8, pp. 922-933, 2013.

[5] M. Martinez-Perez, A. Highes, A. Stanton, S. Thorn, N. Chapman, A. Bharath and K. Parker, "Retinal vascular tree morphology: a semi-automatic quantification", IEEE Transactions on Biomedical Engineering, vol. 49, no. 8, pp. 912-917, 2002.

[6] E. Grisan, M. Foracchia and A. Ruggeri, "A Novel Method for the Automatic Grading of Retinal Vessel Tortuosity", IEEE Transactions on Medical Imaging, vol. 27, no. 8, pp. 310-319, 2008.

[7] C. Heneghan, "Characterization of changes in blood vessel width and tortuosity in retinopathy of prematurity using image analysis", Medical Image Analysis, vol. 6, no. 4, pp. 407-429, 2002.

[8] S. Chaudhuri, S. Chatterjee, N. Katz, M. Nelson and M. Goldbaum, "Detection of blood vessels in retinal images using two-dimensional matched filters", IEEE Transactions on Medical Imaging, vol. 8, no. 3, pp. 263-269, 1989.

[9] M. E. Martínez-Pérez, A. D. Hughes, A. V. Stanton, S. A. Thom, A. A. Bharath, and K. H. Parker, “Retinal Blood Vessel Segmentation by Means of Scale-Space Analysis and Region Growing,” Medical Image Computing and Computer-Assisted Intervention – MICCAI’99 Lecture Notes in Computer Science, Springer Berlin Heidelberg, pp. 90–97, 1999.

[10] A. Hoover, V. Kouznetsova, and M. Goldbaum, “Locating blood vessels in retinal images by piecewise threshold probing of a matched filter response,” IEEE Transactions on Medical Imaging IEEE Trans. Med. Imaging, vol. 19, no. 3, pp. 203–210, 2000.

[11] F. Zana and J.-C. Klein, “Segmentation of vessel-like patterns using mathematical morphology and curvature evaluation,” IEEE Transactions on Image Processing IEEE Trans. on Image Process., vol. 10, no. 7, pp. 1010–1019, 2001.

[12] X. Jiang and D. Mojon, “Adaptive local thresholding by verification-based multithreshold probing with application to vessel detection in retinal images,” IEEE Transactions on Pattern Analysis and Machine Intelligence IEEE Trans. Pattern Anal. Machine Intell., vol. 25, no. 1, pp. 131–137, 2003.

[13] K. Vermeer, F. Vos, H. Lemij, and A. Vossepoel, “A model based method for retinal blood vessel detection,” Computers in Biology and Medicine, vol. 34, no. 3, pp. 209–219, 2004

[14] M. Fraz, S. Barman, P. Remagnino, A. Hoppe, A. Basit, B. Uyyanonvara, A. Rudnicka, and C. Owen, “An approach to localize the retinal blood vessels using bit planes and centerline detection,” Computer Methods and Programs in Biomedicine, vol. 108, no. 2, pp. 600–616, 2012.

[15] A. Mendonca and A. Campilho, “Segmentation of retinal blood vessels by combining the detection of centerlines and morphological reconstruction,” IEEE Transactions on Medical Imaging IEEE Trans. Med. Imaging, vol. 25, no. 9, pp. 1200–1213, 2006.

[16] M. Al-Rawi, M. Qutaishat, and M. Arrar, “An improved matched filter for blood vessel detection of digital retinal images,” Computers in Biology and Medicine, vol. 37, no. 2, pp. 262–267, 2007.

[17] M. E. Martinez-Perez, A. D. Hughes, S. A. Thom, A. A. Bharath, and K. H. Parker, “Segmentation of blood vessels from red-free and fluorescein retinal images,” Medical Image Analysis, vol. 11, no. 1, pp. 47–61, 2007.

[18] M. E. Martinez-Perez, A. D. Hughes, S. A. Thom, and K. H. Parker, “Improvement of a retinal blood vessel segmentation method using the Insight Segmentation and Registration Toolkit (ITK),” Annual International Conference of the IEEE Engineering in Medicine and Biology Society, vol. 29, pp. 892-895, 2006.

[19] L. Wang, A. Bhalerao, and R. Wilson, “Analysis of Retinal Vasculature Using a Multiresolution Hermite Model,” IEEE Transactions on Medical Imaging IEEE Trans. Med. Imaging, vol. 26, no. 2, pp. 137–152, 2007.

[20] L. Espona, M. J. Carreira, M. Ortega, and M. G. Penedo, “A Snake for Retinal Vessel Segmentation,” Pattern Recognition and Image Analysis Lecture Notes in Computer Science, Springer Berlin Heidelberg, pp. 178–185, 2007.

[21] Y. Yang, S. Huang, and N. Rao, “An Automatic Hybrid Method for Retinal Blood Vessel Extraction,” International Journal of Applied Mathematics and Computer Science, vol. 18, no. 3, pp. 399-407, 2008.

[22] A. Anzalone, F. Bizzarri, M. Parodi, and M. Storace, “A modular supervised algorithm for vessel segmentation in red-free retinal images,” Computers in Biology and Medicine, vol. 38, no. 8, pp. 913–922, 2008.

[23] D. Farnell, F. Hatfield, P. Knox, M. Reakes, S. Spencer, D. Parry, and S. Harding, “Enhancement of blood vessels in digital fundus photographs via the application of multiscale line operators,” Journal of the Franklin Institute, vol. 345, no. 7, pp. 748–765, 2008.

[24] B. Lam and H. Yan, “A Novel Vessel Segmentation Algorithm for Pathological Retina Images Based on the Divergence of Vector Fields,” IEEE Transactions on Medical Imaging IEEE Trans. Med. Imaging, vol. 27, no. 2, pp. 237–246, 2008.

[25] L. Espona, M. Carreira, M. Penedo, and M. Ortega, “Retinal vessel tree segmentation using a deformable contour model,” International Conference on Pattern Recognition, vol. 19, pp. 1-4, 2008.

[26] M. Vlachos and E. Dermatas, “Multi-scale retinal vessel segmentation using line tracking,” Computerized Medical Imaging and Graphics, vol. 34, no. 3, pp. 213–227, 2010.

[27] B. Al-Diri, A. Hunter, and D. Steel, “An Active Contour Model for Segmenting and Measuring Retinal Vessels,” IEEE Transactions on Medical Imaging IEEE Trans. Med. Imaging, vol. 28, no. 9, pp. 1488–1497, 2009.

[28] C. Muramatsu, Y. Hatanaka, T. Iwase, T. Hara, and H. Fujita, “Automated detection and classification of major retinal vessels for determination of diameter ratio of arteries and veins,” Medical Imaging 2010: Computer-Aided Diagnosis, vol. 7624, no.1, pp. 1-8, 2010.

[29] J. Ng, S. Clay, S. Barman, A. Fielder, M. Moseley, K. Parker, and C. Paterson, “Maximum likelihood estimation of vessel parameters from scale space analysis,” Image and Vision Computing, vol. 28, no. 1, pp. 55–63, 2010.

[30] M. A. Amin and H. Yan, “High speed detection of retinal blood vessels in fundus image using phase congruency,” Soft Computing, vol. 15, no. 6, pp. 1217–1230, 2010.

[31] K. K. Delibasis, A. I. Kechriniotis, C. Tsonos, and N. Assimakis, “Automatic model-based tracing algorithm for vessel segmentation and diameter estimation,” Computer Methods and Programs in Biomedicine, vol. 100, no. 2, pp. 108–122, 2010.

[32] M. S. Miri and A. Mahloojifar, “Retinal Image Analysis Using Curvelet Transform and Multistructure Elements Morphology by Reconstruction,” IEEE Transactions on Biomedical Engineering IEEE Trans. Biomed. Eng., vol. 58, no. 5, pp. 1183–1192, 2011.

[33] F. Rossant, M. Badellino, A. Chavillon, I. Bloch, and M. Paques, “A Morphological Approach for Vessel Segmentation in Eye Fundus Images, with Quantitative Evaluation,” Journal of Medical Imaging and Health Informatics, vol. 1, no. 1, pp. 42–49, Jan. 2011.

[34] M. M. Fraz, P. Remagnino, A. Hoppe, B. Uyyanonvara, A. R. Rudnicka, C. G. Owen, and S. A. Barman, “An Ensemble Classification-Based Approach Applied to Retinal Blood Vessel Segmentation,” IEEE Transactions on Biomedical Engineering IEEE Trans. Biomed. Eng., vol. 59, no. 9, pp. 2538–2548, 2012.

[35] Y. Xu, T. Géraud, and L. Najman, “Two Applications of Shape-Based Morphology: Blood Vessels Segmentation and a Generalization of Constrained Connectivity,” Lecture Notes in Computer Science Mathematical Morphology and Its Applications to Signal and Image Processing, Springer Berlin Heidelberg, pp. 390–401, 2013.

[36] Y. Wang, G. Ji, P. Lin, and E. Trucco, “Retinal vessel segmentation using multiwavelet kernels and multiscale hierarchical decomposition,” Pattern Recognition, vol. 46, no. 8, pp. 2117–2133, 2013.

[37] A. Salazar-Gonzalez, D. Kaba, Y. Li, and X. Liu, “Segmentation of the Blood Vessels and Optic Disk in Retinal Images,” IEEE Journal of Biomedical and Health Informatics, vol. 18, no. 6, pp. 1874–1886, 2014.

[38] T. Chakraborti, D. K. Jha, A. S. Chowdhury, and X. Jiang, “A self-adaptive matched filter for retinal blood vessel detection,” Machine Vision and Applications, vol. 26, no. 1, pp. 55–68, 2014.

[39] S. Wang, Y. Yin, G. Cao, B. Wei, Y. Zheng, and G. Yang, “Hierarchical retinal blood vessel segmentation based on feature and ensemble learning,” Neurocomputing, vol. 149, no. 3, pp. 708–717, 2015.

[40] W. S. Oliveira, T. I. Ren, and G. D. C. Cavalcanti, “An Unsupervised Segmentation Method for Retinal Vessel Using Combined Filters,” IEEE 24th International Conference on Tools with Artificial Intelligence, vol. 1, pp. 750-756, 2012.

[41] D. Ortiz, M. Cubides, A. Suarez, M. Zequera, J. Quiroga, J. Gomez, and N. Arroyo, “Support system for the preventive diagnosis of Hypertensive Retinopathy,” 2010 Annual International Conference of the IEEE Engineering in Medicine and Biology, vol. 1, pp. 5649-5652, 2010.

[42] K. Narasimhan, V. Neha, and K. Vijayarekha, “Hypertensive Retinopathy Diagnosis from Fundus Images by Estimation of Avr,” Procedia Engineering, vol. 38, no.1, pp. 980–993, 2012.

[43] C. Agurto, V. Joshi, S. Nemeth, P. Soliz, and S. Barriga, “Detection of hypertensive retinopathy using vessel measurements and textural features,” Annual International Conference of the IEEE Engineering in Medicine and Biology Society, vol. 36, pp. 5406-5409, 2014.

[44] A. Ruggeri, E. Grisan, and M. D. Luca, “An automatic system for the estimation of generalized arteriolar narrowing in retinal images,” Annual International Conference of the IEEE Engineering in Medicine and Biology Society, vol. 29, pp. 6463-6466, 2007.

[45] G.C. Manikis, V. Sakkalis, X. Zabulis, P. Karamaounas, A.Triantafyllou, S. Douma, C. Zamboulis, K.Marias, "An image analysis framework for the early assessment of hypertensive retinopathy signs." E-Health and Bioengineering Conference (EHB) IEEE, vol.1, pp. 1-6, 2011.

[46] C. Muramatsu, Y. Hatanaka, T. Iwase, T. Hara and H. Fujita, "Automated selection of major arteries and veins for measurement of arteriolar-to-venular diameter ratio on retinal fundus images", Computerized Medical Imaging and Graphics, vol. 35, no. 6, pp. 472-480, 2011.

[47] S. Khitran, M. Akram, A. Usman and U. Yasin, "Automated system for the detection of hypertensive retinopathy", International Conference on Image Processing Theory, Tools and Applications (IPTA), vol. 4, pp. 1-6, 2014.

[48] H. Li, W. Hsu, M. Lee, and T. Wong, “Automatic Grading of Retinal Vessel Caliber,” IEEE Transactions on Biomedical Engineering IEEE Trans. Biomed. Eng., vol. 52, no. 7, pp. 1352–1355, 2005

[49] N. Chapman, G. Dell’Omo, M. S. Sartini, N. Witt, A. Hughes, S. Thom, and R. Pedrinelli, “Peripheral vascular disease is associated with abnormal arteriolar diameter relationships at bifurcations in the human retina,” Clinical Science, vol. 103, no. 2, pp. 111-116, 2002.

[50] H. Shen, C. Stewart, B. Roysam, G. Lin, and H. Tanenbaum, “Frame-rate spatial referencing based on invariant indexing and alignment with application to online retinal image registration,” IEEE Transactions on Pattern Analysis and Machine Intelligence IEEE Trans. Pattern Anal. Machine Intell., vol. 25, no. 3, pp. 379–384, 2003.

[51] C.L. Tsai, C. Stewart, H. Tanenbaum, and B. Roysam, “Model-Based Method for Improving the Accuracy and Repeatability of Estimating Vascular Bifurcations and

Crossovers From Retinal Fundus Images," IEEE Transactions on Information Technology in Biomedicine IEEE Trans. Inform. Technol. Biomed., vol. 8, no. 2, pp. 122–130, 2004.

[52] B. Al-Diri and A. Hunter, "Automated Measurements of Retinal Bifurcations," IFMBE Proceedings World Congress on Medical Physics and Biomedical Engineering, vol. 1, no.11, pp. 205–208, 2009.

[53] NK El Abbadi, EH El Saadi, "Automatic detection of vascular bifurcations and crossovers in retinal fundus image," International Journal of Computer Science Issues (IJCSI), vol.19, no. 2, pp. 178-181, 2013.

[54] H. Shen, B. Roysam, C. Stewart, J. Turner, and H. Tanenbaum, "Optimal scheduling of tracing computations for real-time vascular landmark extraction from retinal fundus images," IEEE Transactions on Information Technology in Biomedicine, vol. 5, no.1, pp. 77–91, 2001.

[55] T. Chanwimaluang and G. Fan, "An efficient blood vessel detection algorithm for retinal images using local entropy thresholding," Proceedings of the 2003 International Symposium on Circuits and Systems, vol. 5, no.3, pp. 21-24, 2003.

[56] El. Abbadi, El. Saadi, "Automatic Retinal Vessel Tortuosity Measurement," Journal of Computer Science, vol. 9, no. 11, pp. 1456–1460, 2013.

[57] D. Onkaew, R. Turior, B. Uyyanonvara, N. Akinori, and C. Sinthanayothin, "Automatic retinal vessel tortuosity measurement using curvature of improved chain code," International Conference on Electrical, Control and Computer Engineering (InECCE), vol. 1, pp. 183-186, 2011.

[58] L. Zhou, M. Rzeszotarski, L. Singerman, and J. Chokreff, "The detection and quantification of retinopathy using digital angiograms," IEEE Transactions on Medical Imaging IEEE Trans. Med. Imaging, vol. 13, no. 4, pp. 619–626, 1994.

[59] A. Kaupp, H. Toonen, S. Wolf, K. Schulte, R. Effert, D. Meyer-Ebrecht, M. Reim, "Automatic evaluation of retinal vessel width and tortuosity in digital fluorescein angiograms," Investigative Ophthalmology & Visual Science, vol. 32, no. 4, pp. 863-86, 1991.

[60] O. Smedby, N. Hogman, S. Nilsson, U. Erikson, A.G. Olsson, G. Walldius, "Two-dimensional tortuosity of the superficial femoral artery in early atherosclerosis," Journal of Vascular Research, vol. 30, no. 4, pp. 181–191, 1993.

[61] J. J. Capowski, J. A. Kylstra, and S. F. Freedman, "A Numeric Index Based On Spatial Frequency For The Tortuosity Of Retinal Vessels And Its Application To Plus Disease In Retinopathy Of Prematurity," Retina, vol. 15, no. 6, pp. 490-500, 1995.

[62] DRIVE database. Available at: http://www.isi.uu.nl/Research/Databases/DRIVE/. Accessed 8 July 2015.

[63] STARE database. Available at: http://www.ces.clemson.edu/~ahoover/stare/. Accessed 8 July 2015.

[64] INSPIRE-AVR dataset. Available at: http://www.medicine.uiowa.edu/eye/Datasets/. Accessed 8 July 2015.

[65] MESSIDOR database. Available at: http://www.adcis.net/en/Download-Third-Party/Messidor.html. Accessed 8 July 2015.

[66] RET-TORT dataset. Available at: http://bioimlab.dei.unipd.it/Retinal%20Vessel%20Tortuosity.htm. Accessed 8 July 2015.

[67] D. Youssef and N. H. Solouma, "Accurate detection of blood vessels improves the detection of exudates in color fundus images," Computer Methods and Programs in Biomedicine, vol. 108, pp. 1052–1061, 2012.

[68] J. Kaur, D. Mittal, "Segmentation and Measurement of Exudates in Fundus Images of the Retina for Detection of Retinal Disease," Journal of Biomedical Engineering and Medical Imaging, vol. 2, no. 3, pp. 27-38, 2015.

[69] K. Kumari, D. Mittal, "Automated drusen detection technique for age-related macular degeneration," Journal of Biomedical Engineering and Medical Imaging, vol. 2, no. 1, pp. 18-26, 2015.

[70] A. Rani, D. Mittal, "Measurement of Arterio-Venous Ratio for Detection of Hypertensive Retinopathy through Digital Color Fundus Images," Journal of Biomedical Engineering and Medical Imaging, vol. 2, no. 5, pp. 35-45, 2015.

[71] C. Sinthanayothin, J. F. Boyce, H. L. Cook, and T. H. Williamson, "Automated localisation of the optic disc, fovea, and retinal blood vessels from digital colour fundus images," British Journal of Ophthalmology, vol. 83, no. 8, pp. 902–910, 1999.

[72] M. Niemeijer, X. Xu, A. V. Dumitrescu, P. Gupta, B. V. Ginneken, J. C. Folk, and M. D. Abramoff, "Automated Measurement of the Arteriolar-to-Venular Width Ratio in Digital Color Fundus Photographs," IEEE Transactions on Medical Imaging IEEE Trans. Med. Imaging, vol. 30, no. 11, pp. 1941–1950, 2011.

[73] K. Kumari, D. Mittal, "Drusen Quantification for Early Identification of Age Related Macular Degeneration," Advances in Image and Video Processing AIVP, vol. 3, no. 3, pp. 28-40, 2015.

[74] N. Witt, T. Y. Wong, A. D. Hughes, N. Chaturvedi, B. E. Klein, R. Evans, M. Mcnamara, S. A. M. Thom, and R. Klein, "Abnormalities of Retinal Microvascular Structure and Risk

of Mortality From Ischemic Heart Disease and Stroke," Hypertension, vol. 47, no. 5, pp. 975–981, Mar. 2006.

[75] D. Mittal and K. Kumari, "Automated detection and segmentation of drusen in retinal fundus images," Computers & Electrical Engineering, vol. 47, no. 2, pp. 82–95, 2015.

[76] J. Parr and G. Spears, "General Caliber of the Retinal Arteries Expressed as the Equivalent width of the Central Retinal Artery," American Journal of Ophthalmology, vol. 77, no. 4, pp. 472–477, 1974.

[77] M. D. Knudtson, K. E. Lee, L. D. Hubbard, T. Y. Wong, R. Klein, and B. E. Klein, "Revised formulas for summarizing retinal vessel diameters," Current Eye Research, vol. 27, no. 3, pp. 143–149, 2003.

[78] J. Parr and G. Spears, "Mathematic Relationships Between the width of a Retinal Artery and the Widths of its Branches," American Journal of Ophthalmology, vol. 77, no. 4, pp. 478–483, 1974.

[79] L. D. Hubbard, R. J. Brothers, W. N. King, L. X. Clegg, R. Klein, L. S. Cooper, A. Sharrett, M. D. Davis, and J. Cai, "Methods for evaluation of retinal microvascular abnormalities associated with hypertension/sclerosis in the atherosclerosis risk in communities study," Ophthalmology, vol. 106, no. 12, pp. 2269–2280, 1999

[80] C. D. Murray, "The Physiological Principle Of Minimum Work Applied To The Angle Of Branching Of Arteries," The Journal of General Physiology, vol. 9, no. 6, pp. 835–841, 1926.

[81] M. Zamir, "Arterial bifurcations in the human retina," The Journal of General Physiology, vol. 74, no. 4, pp. 537–548, 1979.

[82] W. E. Hart, M. Goldbaum, B. Cote, P. Kube, and M. R. Nelson, "Measurement and classification of retinal vascular tortuosity," International Journal of Medical Informatics, vol. 53, no. 2, pp. 239–252, 1999.

[83] W. Lotmar, A. Freiburghaus, and D. Bracher, "Measurement of vessel tortuosity on fundus photographs," Ophthalmology, vol. 211, no. 1, pp. 49–57, 1979.

[84] M. Zamir, "Optimality principles in arterial branching," Journal of Theoretical Biology, vol. 62, no. 1, pp. 227–251, 1976.

LIST OF PUBLICATIONS

[1] A. Rani, D. Mittal, "Measurement of Arterio-Venous Ratio for Detection of Hypertensive Retinopathy through Digital Color Fundus Images," Journal of Biomedical Engineering and Medical Imaging, vol. 2, no.5, pp. 35-45, 2015.

[2] A. Rani, D. Mittal, R. Sunkaria, "An Improved Method for the Detection of Retinal Blood Vasculature in Computer-Aided Diagnosis of Hypertensive Retinopathy," 2016 IEEE First International Conference on Power Electronics, Intellegent control and Energy Systems (IEEE ICPEICES 2016) . (Presented)

[3] A. Rani, D. Mittal, R. Sunkaria, "Measurement of Bifurcation Features in Retinal Fundus Images," India International Conference on Image Processing (IEEE IICIP 2016). (Accepted)

[4] A. Rani, D. Mittal, "Detection of Hypertensive Retinopathy with Automated Segmentation of Blood Vessels in Retinal Fundus Images," Image and Vision Computing. (Communicated)

Anju_Thesis

ORIGINALITY REPORT

19%	8%	17%	4%
SIMILARITY INDEX	INTERNET SOURCES	PUBLICATIONS	STUDENT PAPERS

PRIMARY SOURCES

1	Fraz, M.M., S.A. Barman, P. Remagnino, A. Hoppe, A. Basit, B. Uyyanonvara, A.R. Rudnicka, and C.G. Owen. "An approach to localize the retinal blood vessels using bit planes and centerline detection", Computer Methods and Programs in Biomedicine, 2012. Publication	3%
2	scholarpublishing.org Internet Source	2%
3	Mittal, Deepti, and Kajal Kumari. "Automated detection and segmentation of drusen in retinal fundus images", Computers & Electrical Engineering, 2015. Publication	1%
4	Niemeijer, M., Xiayu Xu, A. V. Dumitrescu, P. Gupta, B. van Ginneken, J. C. Folk, and M. D. Abramoff. "Automated Measurement of the Arteriolar-to-Venular Width Ratio in Digital Color Fundus Photographs", IEEE Transactions on Medical Imaging, 2011. Publication	1%